Deep Transfer-Learning Based Lithium-Ion Battery Fault Diagnosis

by

Chukwuemeka Nelson Nwauche

A thesis submitted to the
School of Graduate and Postdoctoral Studies in partial
fulfillment of the requirements for the degree of

Master of Applied Science in Automotive Engineering

Department of Automotive, Mechanical and Manufacturing Engineering

School of Graduate and Postdoctoral Studies

The Faculty of Engineering and Applied Science

Ontario Tech University

Oshawa, Ontario, Canada

August 2022

THESIS EXAMINATION INFORMATION

Submitted by: **Chukwuemeka Nelson Nwauche**

Master of Applied Science in **Automotive Engineering**

Thesis title:
Deep Transfer Learning Based Lithium-Ion Battery Fault Diagnosis

An oral defense of this thesis took place on August 8, 2022, in front of the following examining committee:

Examining Committee:

Chair of Examining Committee	Martin Agelin-Chaab
Research Supervisor	Xianke Lin
Examining Committee Member	Jing Ren
Thesis Examiner	Ramona Fayazfar

The above committee determined that the thesis is acceptable in form and content and that a satisfactory knowledge of the field covered by the thesis was demonstrated by the candidate during an oral examination. A signed copy of the Certificate of Approval is available from the School of Graduate and Postdoctoral Studies.

ABSTRACT

Fault detection in lithium-ion batteries (LiB) is paramount to ensuring the long life and proper functioning of the batteries. To that end, this thesis proposes a combined fault diagnosis framework that leverages voltage charging curves and voltage charging curve fault residuals to accurately detect multiple faults within a LIB during partial and full charging regimes. This framework removes the need for parameter tuning and is also adaptable to varying battery chemistries and performs well with a small amount of available data. The framework leverages voltage residuals generated via a randomly initialized or pre-trained LSTM (Long Short Term Memory) model. Experimental results show its ability to accurately detect the different types of faults utilizing full voltage charging curve residuals with an accuracy of 95%. The framework can also detect faults utilizing partial voltage charging curve residuals & a pre-trained LSTM model with an accuracy of 94%.

Keywords: Lithium-ion batteries, Transfer Learning, Convolutional Neural Networks, Electric Vehicles, Battery Fault Diagnosis

AUTHOR'S DECLARATION

I hereby declare that this thesis consists of original work which I have authored. This is a true copy of the thesis, including any required final revisions, as accepted by my examiners.

I authorize the University of Ontario Institute of Technology (Ontario Tech University) to lend this thesis to other institutions or individuals for the purpose of scholarly research. I further authorize the University of Ontario Institute of Technology (Ontario Tech University) to reproduce this thesis by photocopying or by other means, in total or in part, at the request of other institutions or individuals for the purpose of scholarly research. I understand that my thesis will be made electronically available to the public.

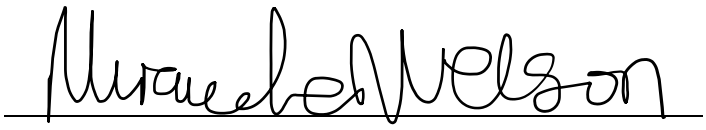

CHUKWUEMEKA NELSON NWAUCHE

STATEMENT OF CONTRIBUTIONS

Part of the work described in Chapter 7 has been published as:

C. N. Nwauche, X. Lin, “Fault Diagnosis of a Single Battery Cell Via Transfer Learning”, *13th International Green Energy Conference (IGEC-XIII)*

C. N. Nwauche, X. Lin, “Lithium-ion Battery Multi-Fault Diagnosis via Transfer Learning Based LSTM and Convolutional Neural Networks”, *14th International Green Energy Conference (IGEC-XIV)*

ACKNOWLEDGEMENTS

I would like to thank my family for their support throughout this process and my supervisor, Dr. Xianke Lin, for his guidance during the development of this thesis.

TABLE OF CONTENTS

LIST OF TABLES

CHAPTER 4

CHAPTER 5

LIST OF FIGURES

CHAPTER 1

CHAPTER 3

CHAPTER 4

CHAPTER 5

LIST OF ABBREVIATIONS AND SYMBOLS

LiB	Lithium ion Batteries
CNNs	Convolutional Neural Networks
LSTMs	Long Short Term Memory neural networks
RES152	ResNet 152 convolutional neural network

Outline

The thesis is organized as follows:

In Chapter 1 a brief introduction is presented. In Chapter 2, the details of the conducted literature review are covered. In Chapter 3, a theoretical background of LSTM and CNN neural networks and transfer learning are covered. Chapter 4 covers the methodology of the research project and Chapter 5 covers the results and their subsequent discussion followed by a brief conclusion in Chapter 6 summarizing the thesis and discussing future works.

- **Chapter 1 Introduction** presents background information about LIBs and various fault diagnosis techniques. Also, the objectives, assumptions, and contributions of this thesis are presented.
- **Chapter 2 Literature Review** reviews existing LIB fault diagnosis literature and the research gaps that this thesis addresses are articulated and presented.

  Chapter 3 Background discusses the LSTM and CNN neural networks as well as transfer learning. With regards to LSTMs and CNNs, the structure and mode of operation are discussed in detail followed by a discussion of transfer learning in terms of its mode of operation, advantages, disadvantages, and a literature review within the context of LIBs
- **Chapter 4 Methodology** presents the fault diagnosis problem to be solved and discusses the battery manager used for data collection and the various techniques used to optimize the RES152 technique used for fault detection.

- **Chapter 5 Results and Discussion** presents the results of the conducted studies using plain partial voltage charging curves and voltage residuals followed by a discussion of the results.
- **Chapter 6 Conclusion and Future Works** concludes the current work and suggest future works to be done.

Chapter 1. Introduction

1.1 Background

The turn of the 21st century has seen a rise in interest in cleaner energy sources to replace fossil fuels. Lithium-ion batteries (LiB) are one of these new clean energy sources that have seen applications in various industries such as automotive, industrial, and commercial energy industries. Although a new and interesting technology with various applications, LiB is still prone to failure due to varying operating and manufacturing conditions. As such, the need to create fault diagnosis systems that can detect a wide range of faults under a wide range of conditions becomes apparent. This need to detect these faults is a result of the high potential for loss of life and/or property when said faults occur. Also, the occurrence of LiB faults is usually accompanied by fire and/or toxic fumes making the early detection of faults paramount. Figure 1.1 shows an overview of the different types of faults. LiB faults can be categorized into external and internal faults. In this thesis, we focus on internal faults but review the literature from both types of faults to ensure completeness. With regards to internal faults, these are the faults that occur inside the battery and their presence either degrades or leads to the accelerated degradation of the battery. External faults refer to those faults that occur in the associated sensors and maintenance devices such as cooling systems of batteries and battery packs. Internal faults are the main focus of this thesis because their occurrence has a higher associated risk. The occurrence of an internal fault is usually accompanied by fire, toxic fumes, and/or explosions. As such, their occurrence is very dangerous. For both internal and external faults, algorithms

have been developed to aid in the detection of these faults. Figure 1.2 shows the different types of algorithms that are present in the literature. Fault diagnosis algorithms can be broadly divided into model and non-model-based [1]. Model-based algorithms, as the name implies, utilize different types of models including physics-based and statistical models to predict the behavior of a healthy or faulty battery depending on the specific model used. Model-based techniques can be divided into four categories, namely parity space, parameter estimation, structural analysis, and state estimation. State estimation can be divided into filter and observer techniques. Parity space techniques involve detecting faults via the generation of residuals from the input and output relationship that a model and the corresponding experimental measurements will have. Parameter estimation involves the estimation of the model parameters based on measurements and a fault is then detected when there is a change in the estimated value. Structural analysis involves the identification of faults via the analysis which is a structural model of the battery system. Finally, state estimation involves the detection of faults via the generation of residuals using filters and/or observers to generate estimations which are then compared with the actual measured value. A fault is detected when a certain threshold for the estimation is exceeded.

Non-model-based algorithms utilize raw data collected from attached sensors and/or features extracted from the collected raw data to infer the health of the battery and/or battery pack. It can be divided into signal-processing techniques and knowledge-based techniques.

Signal processing techniques involve transforming the measured data into some fault parameters such as correlation coefficient or entropy. The fault detection is via the

detection of an abnormality in the parameters. Knowledge-based techniques utilize the knowledge obtained from measured data to generate rules about the regular operation and the faults are detected when the measured data deviates from the rules generated by the technique.

The proposed technique in this thesis is a non-model-based, knowledge-based, Artificial Neural Network (ANN) technique that leverages transfer learning to overcome the high data requirements of knowledge-based techniques. The primary criticism of knowledge-based techniques is the data requirements needed to train the model effectively. The technique developed in this thesis addresses this issue via transfer learning. Transfer learning is a technique by which a model is trained on a source domain dataset with a large amount of data and then used on a target domain dataset which may have the same data format but encodes different information. Another contribution of this work is the use of partial voltage curves for fault detection. Most knowledge-based algorithms utilize full voltage charging curves. However, to closer mimic consumer usage of such devices, partial voltage curves were used. The third contribution of this work is the ability of the network to be used on varying battery chemistries. The development of a technique that can work with more battery chemistries with a small amount of data from said batteries is beneficial because it allows for the development of an adaptable fault diagnosis system. The fault diagnosis system can be deployed and slowly fine-tuned over time as more fault data for that specific battery is collected.

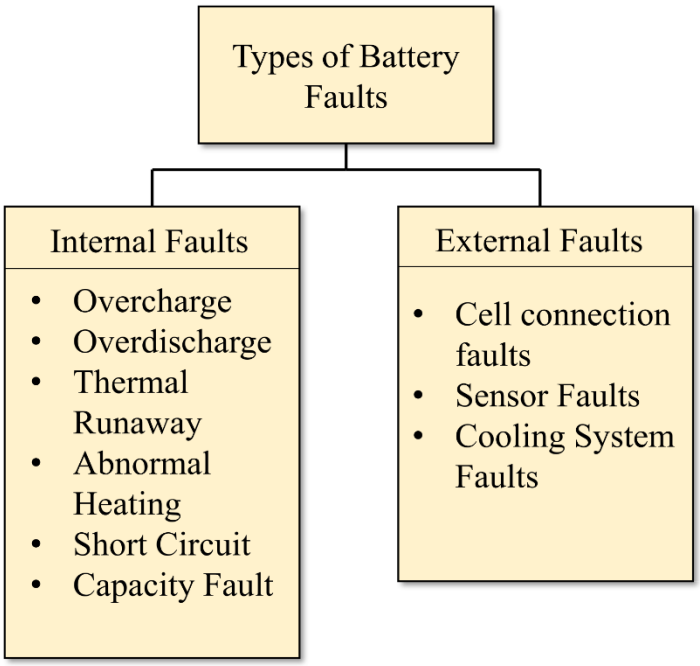

Figure 1.1: Types of Faults[1]

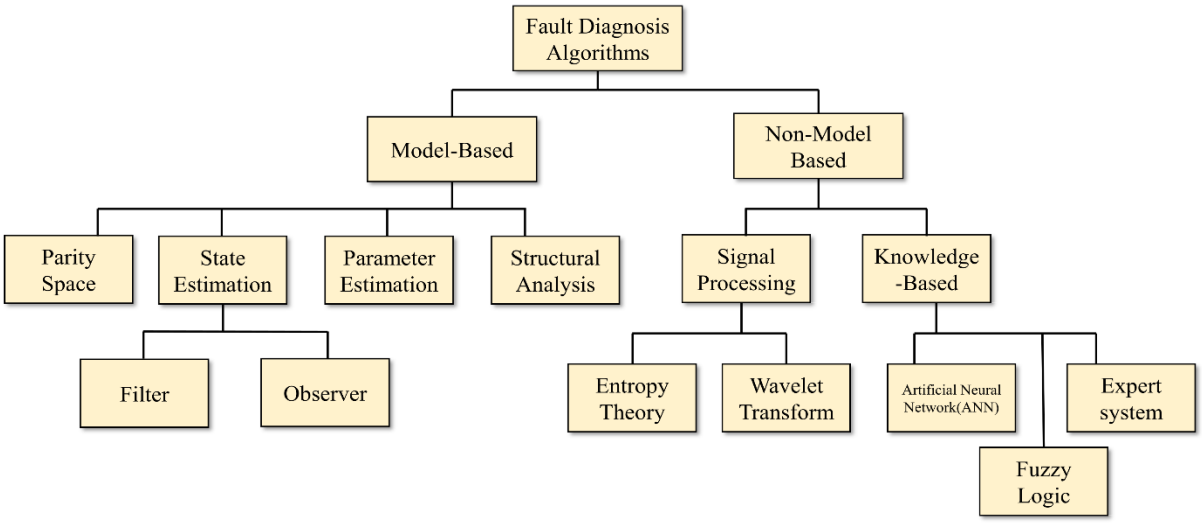

Figure 1.2: Types of Fault Diagnosis Algorithms[2]

1.2 Objectives & Assumptions

The primary goal of this research is to develop a fault diagnosis framework that can be used on various LIBs.

The detailed objectives of this research include:

i. The development of a fault diagnosis framework that can effectively detect thermal faults
ii. The development of a fault diagnosis framework that can effectively detect short circuit faults
iii. The development of a fault diagnosis framework that can effectively detect overcharge faults
iv. The development of a fault diagnosis framework that can leverage graphed voltage charge curves for fault diagnosis
v. The development of a fault diagnosis framework that can leverage graphed voltage charging curve residuals for battery fault diagnosis.

The assumptions made during this research include:

i. Multiple faults do not occur simultaneously.
ii. Electrochemical effects due to variability in manufacturing are negligible.

1.3 Contributions

To the best knowledge of the author, the main contributions of this research are as follows:

i. The development of an offline data-driven fault diagnostic approach that utilizes partial voltage charging curves to predict a fault present in the cell.

ii. A transfer learning-based neural network approach that is low in training data requirements and training time compared to other data-driven approaches as well as requiring no feature engineering.

iii. An offline data-driven fault diagnosis approach that can quickly adapt to varying battery conditions & chemistries via retraining or dataset augmentation.

iv. The development of a combined data-driven and model-based fault detection framework.

v. A scalable and adaptable framework for offline fault detection.

vi. A fault prediction framework that allows for fault detection using both full and partial voltage charging curves.

vii. A fault prediction framework that leverages voltage residuals for fault detection.

1.4 Summary

In this chapter, the model-based LIB fault detection algorithms were first reviewed, followed by a review of the non-model-based LIB fault detection algorithms. Finally, the existing research gaps were pointed out and discussed.

Chapter 2. Literature Review

2.1 Introduction

In this section, the existing literature with regards to LIB fault diagnosis algorithms are reviewed and discussed. Firstly, model-based algorithms are discussed in-depth followed by a discussion of non-model-based algorithms and finally, the research gaps are identified and explained.

2.2 Fault Diagnosis Algorithms Review

In this chapter, the various fault diagnosis algorithms in the literature are discussed, reviewed, and analyzed to determine research gaps that are addressed in this thesis

2.2.1 Model-Based LIBs Fault Diagnosis Algorithms Review

With regards to the current model-based fault diagnosis literature, in [2], the authors detected soft internal short circuit faults via the extraction and analysis of the open-circuit voltage and thus the internal short circuit resistance. The measurement of the internal short circuit resistance can allow for the direct representation of the severity of the fault. Experimental results showed that the error of estimation does not exceed 31.2% and so allows for the early detection of internal short circuit faults. In [3] the authors created a modified multi-scale entropy technique for online fault detection in electric vehicle BMS systems. The technique leverages past electric vehicle drive cycle data and uses said data to extract multi-scale features which are then used for early-

stage fault detection & classification. Real-time experimental results from simulations show the novelty and efficacy of the developed framework. In [4], the authors created an online fault diagnosis technique based on the correlation coefficient method. The technique is combined with a redundant crossed-style measurement circuit and allows for efficient measurement of the voltage in neighboring cells without an accompanying increase in hardware costs. The researchers demonstrated that the technique can avoid false detection of faults and is robust to the variation in various operating conditions including ambient temperature and state-of-charge measurements. In [5], the authors created a fault diagnosis system for current and voltage sensors via the modeling of the battery pack as a hybrid system combined with the leveraging of an unscented particle filter. Results from their experiment showed not only effective state tracking performance but an accurate fault detection capability. In [6], the authors developed a two-step equivalent circuit model. It is used for online detection of external short circuit faults in 18650 form factor NMC (Nickel Manganese Cobalt Oxide) battery packs and cells. Results from their experiments showed that the developed technique can detect the faults in 3.5s. This detection occurs with a less than 25mV terminal voltage error. In [7], the authors created a novel fault diagnosis technique utilizing the interclass correlation coefficient principle. The authors leveraged electric vehicle voltage data to verify the efficacy of this technique. Results from their experiments showed that the novel technique can detect fault signals in electric vehicle voltage data accurately. In [8], the authors accurately detected voltage and temperature sensor faults via the combined use of a Thevenin equivalent circuit model, radial equivalent thermal model, and particle filters. Results from their experiments showed that the developed technique

is capable of accurately detecting thermal faults in battery cells. In [9], the researchers developed a model-based technique for voltage and temperature sensor fault detection via the use of an equivalent circuit model and extended Kalman Filter. It estimates the terminal voltage of the cell and generates residuals which are then used for fault detection. Results from their experiments showed that the proposed technique is capable of accurately detecting both types of faults. In [10], the authors developed a thermal fault diagnosis technique via a distributed parameter thermal model. Their model parametrizes a cylindrical shell battery which is used along with a fault diagnosis framework to detect and estimate the size of present thermal faults. Results from their experiments verified the efficacy of this proposed method. In [11], the authors created an online multi-fault diagnosis framework leveraging modified sample entropy. The technique makes use of a sliding window and is the presence and time of occurrence of a fault. Results from their experiments verified the validity of their proposed technique. In [12], the authors developed a sensor fault detection scheme for electric vehicle battery packs via the use of an extended Kalman Filter. The technique leverages the fact that residuals can be generated from the comparison of actual voltage measurements and voltage prediction. They used the UDD driving cycles dataset to experimentally validate their technique. In [13], the authors proposed an online fault diagnosis framework for the detection of external soft-short circuit faults in series battery packs via the use of a dual extended Kalman filter. Results from their experiments showed the benefits of the technique for the detection of external soft-circuit faults. In [14], Gao et. al developed a model-based technique for the detection of early-stage micro-short circuit faults. The technique makes use of a mean-difference model, an extended

Kalman filter, and a recursive least squares filter. Results from their experiments showed the technique has low computational load as well as accurate fault detection capabilities. In [15], the authors leveraged online capacity estimation to diagnose and differentiate between micro-short circuit faults and low-capacity faults present within a battery pack. Results from their experiments yield promising results and showed the efficacy of the proposed method. In [16], the authors detected sensor faults and located them in battery packs via the use of parameter estimation combined with recursive least squares. The recursive least squares method is used to estimate the parameters of the equivalent circuit model as cell degradation occurs. Results from their experiments validated the efficacy of the method. In [17], Nordmann et. al developed an innovative technique for thermal fault detection and localization that utilizes existent wire harnesses within the battery packs to detect thermal hotspots thus removing the need for the addition of extra thermal sensors. The experimental results validated the technique and provided a promising base for future sensor-less fault detection research. In [18], Zhang et. al proposed an online fault diagnosis scheme for micro short circuit faults in Li-ion cells via the use of the smoothing properties of low-pass filters, a recursive least squares technique, and an equivalent circuit model. The technique was first verified on simulation data and then tested on experimental data collected from cycling cells, verifying the efficacy of the technique. In [19], Lai et. al proposed an online detection framework for internal short circuits via the use of a state-of-charge correlation technique. An extended Kalman Filter was also utilized along with a sliding window correlation coefficient technique to internal short circuits in a cell. Results from their experiments showed the efficacy of the model and fault severity detection capabilities.

In [20], Wei et. al proposed an electrothermal-coupled cylindrical battery model combined with a Lyapunov-based internal resistance estimator to detect various faults such as thermal parameter fault and heat generation. Results from their experiments confirmed the effectiveness of the model for thermal fault detection. In [21], Hashemi et. al developed a fast diagnosis methodology for various faults within battery packs used for electric and hybrid electric aircrafts. The technique relies on health factors that are extracted from models developed to mimic the aforementioned faults. These health factors from the models are then used in identifying faults present within cells during operation of the aircraft. The technique was validated on cell data from a typical flight cycle and confirmed the efficacy of the model. Overall, the model-based approaches have a place in the overall fault diagnosis landscape but the specificity which allows for the excellent fault detection abilities also become a drawback due to the inability of these techniques to be quickly adapted for use outside of the cells for which they were developed. Moreover, they suffer from lack of actual real-world data which may contain information not readily available from modelling.

2.2.2 Non-Model-Based LIBs Fault Diagnosis Algorithms Review

Surveying the current literature for non-model-based techniques, in [22] the authors developed a non-model-based algorithm to predict internal short circuits. The authors extracted features from the full voltage charge-discharge curves of cycled pouch cells and train a random forest classifier, achieving a classification accuracy of 97%. In [23], the authors created a multi-fault diagnostic approach making use of interleaved full

voltage curve measurements and the correlation coefficient method to diagnose internal and sensor faults present in a battery pack. In [24], the authors developed a DBSCAN-based clustering algorithm for detecting thermal runaway faults in individual cells in battery packs based on the full voltage drive cycle curves. Results from their experiments showed the proposed technique can detect potential thermal runaway cells days before the occurrence of the fault. In [25], Yao et al. developed a grid search support vector machine framework utilizing a discrete cosine filtering technique and a modified covariance matrix to detect connection faults within the series battery pack of electric vehicles. In [26], Wang et al. created a fault diagnosis and prognosis system based on the modified Shannon entropy and z-score. A large amount of data from the Service and Management Center for Electric Vehicles (OSMC-EV) in Beijing along with the modified entropy technique is used to predict voltage faults and the z-score technique is used for the prognosis. In [27], Hong et al. proposed an LSTM-based online fault diagnosis framework for electric vehicle battery packs making use of a large amount of data from the OSMC-EV in Beijing. The developed technique has good fault detection capabilities as well as voltage forecasting capabilities but requires a large amount of data for interval training like other data-driven techniques. In [28], the authors proposed an entropy-based fault diagnosis scheme for overvoltage detection in electric vehicle battery packs. The investigation made use of large amounts of pre-processed data from the OSMC-EV in Beijing. Results from the experiments carried out by the researchers validated the technique however like other data-driven techniques reviewed in this thesis, becomes difficult to implement/retrain in the absence of these large amounts of data. In [29], the authors leveraged a state

representation methodology to develop a technique for early voltage fault detection and thermal runaway detection in electric vehicle battery packs. The technique is tested against real-world data from four different electric vehicles and the results verified that it is a novel and effective technique for fault diagnosis. In [30], Hong et. al developed a thermal runaway prognosis technique leveraging utilizing a large amount of data from the OSMC-EV in Beijing. The authors also developed a thermal security management strategy in addition to their prognosis technique and their experimental results validate the approach. In [31], a 3-delta multi-level screening strategy coupled with an optimized neural network is proposed by the authors to monitor cell voltage abnormalities to detect faults present within the battery. Vehicle driving data from a whole year was collected and used to validate the developed technique. The experimental results showed the efficacy of the technique however a major drawback like other data-driven techniques reviewed is the amount of data needed for validation. In [32], the authors utilized a combination of an LSTM neural network, an ECM (Equivalent Circuit Model) model, and a coupling module based on MAB (Modified Adaptive Booster) for online thermal runaway detection. The system is trained on historical voltage drive cycle data and the experimental results showed the efficacy of the proposed model. In [33], the authors developed a radial basis function neural network for the fault diagnosis of various battery faults. Results from the experiments conducted showed near 100% fault detection accuracy; however, the method employed feature generation from collected data. The main drawbacks of the employed technique are the use of feature engineering and the absence of realistic faults used for training the neural network. In [34], the authors proposed a lightweight context-aware fault

diagnosis system-based scheme that leveraged a novel machine-learning algorithm called Extra-Trees for use in detecting various sensor faults. The network is shown to outperform traditional machine learning algorithms like a Support Vector Machine (SVM) and a standard multi-layer perceptron neural network. A criticism of this work is the lack of experimental data as the data used for the study was artificially generated from healthy data. However, the researchers showed that this technique is valid via citations from previously conducted work. In [35], Yao et. al proposed a fault diagnosis scheme based on a wavelet neural network. The technique involved the removal of voltage noise via discrete wavelet transform followed by the creation of various features such as voltage differences. These features are then fed into a general regression neural network. Results from the experiment validated the efficacy of the fault diagnosis scheme in terms of its ability to diagnose the fault and also detection of the severity of the fault. In [36], Zheng et al. proposed a micro-short circuit fault detection strategy reliant on mutual information. The technique accounts for battery degradation and the fault masking effects of the developed faults. The mutual information scheme is capable of accurately differentiating between cells experiencing low capacity vs. cells in which micro-short circuits are occurring. Results from the conducted experiments of the researchers validate the technique. Overall, the non-model-based approaches are an essential component in the overall fault diagnosis landscape but their dependence on large amounts of data and/or feature engineering for extracting useful information from the gathered data are both drawbacks that hinder their efficacy and applicability.

2.2.3 Existing Research Gaps in LIBs Fault Diagnosis Algorithms

A review of the current state-of-the-art machine learning-based fault diagnosis algorithms has been conducted in [37]. It highlights the issues yet to be addressed in the data-driven fault diagnosis literature including lack of training time documentation and generalization ability of developed techniques. Training time documentation refers to measuring the amount of time it takes for machine/deep learning networks to tune their parameters using the data points within the dataset partitioned for training. In this study, the training times for the machine learning algorithms are negligible (<5s) due to the small dataset and so the training times of the deep learning algorithms are what are highlighted in Table 7.2. With regards to the generalization ability, we make that claim based on the experiment carried out on Validation Set 2. Validation Set 2 is comprised of cycling data from a new type of battery cell that is different from the cells used for the training/testing set and Validation Set 1. The network is able to diagnose the faults in this dataset with an accuracy of 75%. This is promising as the network was not trained on data from this dataset. In Validation Set 1, the network is able to detect faults with 85% accuracy. This is also promising since the network has not seen the data during the training or testing phases. Another issue raised in data-driven non-model-based techniques, including machine learning techniques such as [22], is that they utilize various types of features extracted from the voltage/current curves of the battery/battery packs. The disadvantage of this is that any beneficial fault information not captured by these features is lost. As previously stated, feature engineering is the

practice of utilizing various metrics such as statistical (mean, median standard deviation), experiment-specific, and hand-crafted metrics (internal resistance, constant voltage charging time, energy loss etc.) as inputs for machine and deep learning algorithms rather than the raw data from which these features were extracted from. Since the researchers pick what features to generate and use within their model, if a feature that captures relevant data about the fault is not included, the resultant model may not be as accurate compared to a model developed with that feature as one of its inputs. The DLM technique prevents such omissions from happening since it removes the task of feature generation from hands of the researcher. The DLM technique is capable of automatically finding the best features. Moreover, data-driven non-model-based techniques reviewed such as [10] and [11] require vast amounts of data. This becomes a limiting factor in cases where large amounts of training data are not readily available. Finally, many reviewed offline non-model-based data-driven fault prediction techniques utilize the full voltage charge/discharge curve directly or indirectly via feature engineering, where applicable. To the best of the author's knowledge, no attempts have been made to use partial voltage charging curves for fault diagnosis. The use of partial voltage curves is of importance because of the real-life usage patterns of battery-powered devices such as consumer electronics and electric-powered vehicles. Consumers usually do not wait until full discharge before they charge their devices. As such an investigation into fault diagnosis during partial charge is necessary to account for this use case. This thesis addresses this gap by being the first to use the partial charging curves of a cycled LiB to develop an offline data-driven non-model-based technique that can accurately predict the fault present within the LiB battery cell.

2.3 Summary

In this chapter, the model-based LIB fault detection algorithms were first reviewed, followed by a review of the non-model-based LIB fault detection algorithms. Finally, the existing research gaps were pointed out and discussed.

Chapter 3.Background

3.1 LSTMs

Long Short Term Memory neural networks are a subset of Recurrent Neural Networks (RNNs) which in turn are a subset of Artificial Neural Networks that are broadly classified under the umbrella of deep learning/machine learning [38]. RNNs unlike more traditional neural networks like Multi-Layer Perceptron(MLP) and Convolutional Neural Networks(CNNs) can handle sequential data. This makes them prime candidates for various forecasting activities including but not limited to time series forecasting, language translation, and also text-to-speech applications. LSTMs were introduced to address the shortcomings of RNNs which were primarily the vanishing and exploding gradient issues[39]. Figure 3.1 shows a temporally unfolded LSTM cell where the subscript *t* means the current timestep and the subscript *t-1* refers to the previous timestep. The governing equations for the LSTM cell are shown in (1), where x, C, Q, h, f, I, and o are the input vector, cell state, potential candidates, hidden state, and activations for the forget, input and output gates, respectively. In this thesis, LSTMs are used to generate voltage residuals which are then graphed and used for fault detection.

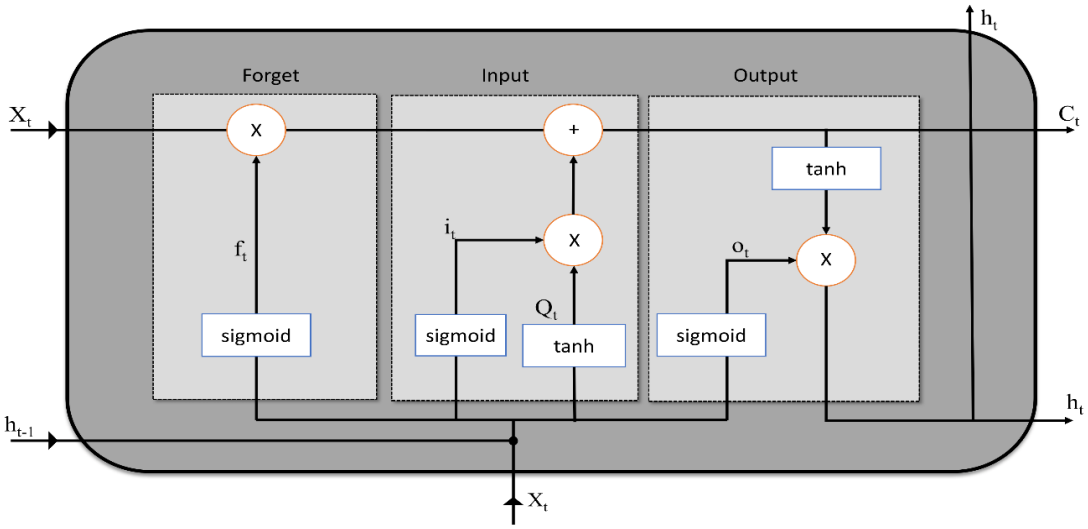

Figure 3.1: LSTM Architecture

$$f_t = sigmoid(W_f h_{t-1} + W_f x_t + b_f)$$

$$i_t = sigmoid(W_i h_{t-1} + W_i x_t + b_i)$$

$$o_t = sigmoid(W_o h_{t-1} + W_o x_t + b_o) \quad (1)$$

$$Q_t = sigmoid(W_Q h_{t-1} + W_Q x_t + b_Q)$$

$$C_t = (f_t C_{t-1} + i_t Q_t)$$

$$h_t = (o_t * \tanh(C_t)$$

3.2 CNNs

Convolutional Neural Networks(CNNs) are another type of Artificial Neural Network that is used in various artificial intelligence tasks including image recognition [39, 40]. CNNs have seen a resurgence since the introduction of AlexNet[42] in 2012 and within the ILSVRC[43]and subsequent winners have also been from the CNN family displaying the high efficacy of this family of neural networks for image recognition. CNNs are composed of multiple layers some of which are custom however, all CNNs do have the following layers in common. These layers are the convolution layer, a non-linearity layer, and a pooling layer. The goal of the convolution layer is to extract features from the image. The equation for the convolution layer is shown in equation 2.

$$V = \left| \frac{\sum_{i=1}^{n} \left(\sum_{j=1}^{n} f_{ij} d_{ij} \right)}{F} \right| \tag{2}$$

V is the output pixel value, f_{ij} is the coefficient of a convolution kernel at position i,j in the kernel, d_{ij} is the data value of the pixel that corresponds to f_{ij}, F is the sum of the coefficients of the kernel or 1 if the sum is 0 and n is the dimension of the kernel.

The goal of the non-linearity layer is to bound the inputs from the previous layer between pre-defined values. The bounds depend on the actual non-linearity layer used. The most common non-linearity layer is the Rectified Linear Unit(ReLu). The equation for the ReLu layer is shown in (3) where x is the input value to the ReLu function.

$$ReLu(x) = \max(0, x) \tag{3}$$

$$W^2 = (W^1 - F)/S + 1$$
$$H^2 = (H^1 - F)/S + 1 \quad (4)$$
$$D^2 = D^1$$

Finally, the pooling layer is used to reduce the dimensionality/ spatial size of the inputs to layers either to help address the vanishing gradient problem or due to some peculiarities such as a change in dimension of the next layers that the inputs may be fed into. The formula for the pooling layer is shown in (4), where W^1 and W^2 are the input and output widths respectively, H^1 and H^2 are the input and output heights, D^1 and D^2 are the input and output depths respectively, F is the kernel size and S is the stride length.

In this thesis, the CNN that is used is called ResNet (Residual Network) 152. It is part of a family of CNNs called Residual Networks. Th underpinning techniques that make ResNets a viable candidate for image recognition are the residual block and skip connections. The two techniques allow information about the image to propagate deeper into the network. Traditional fully connected deep neural networks suffer from this issue of not enough information about the images being able to propagate to the deeper layer of the network. ResNet solve this issue allowing for the utilization of all the layers which in turn leads to better image classification performance.

3.3 Transfer Learning

Transfer Learning is a machine learning/deep learning that addresses the lack of data faced by researchers who employ data-driven approaches. The goal of employing transfer learning is to improve the classification ability of the target learner/model by transferring the knowledge gained from training exercises in the source domain by the source learner/model via the values of the parameters, network weights, and biases in the case of neural networks[43, 44]. In recent years, transfer learning has seen greater adoption within the context of battery health management, prognosis, and fault diagnostics. In [46], Che et al. create a transfer learning-based predictive battery health management system via the estimation of the remaining useful life of the cell. An RNN is used as the target estimator. The source domain is previously collected battery data while the target domain is the RUL of the test battery. The experimental results validate the efficacy of the technique. In [47], Ma et. al develop a hybrid transfer learning scheme to predict the remaining useful life of lithium-ion power batteries. The developed technique utilizes an LSTM network along with developing prediction criteria such as long-term degradation rate to select samples from a historical database of formulations for use in the training of another LSTM network used for the actual RUL prediction. The experimental results are promising and validate the work of the researchers. In [48], the authors develop a transfer learning-based state of charge estimator that is robust to variations in ambient temperature. The technique leverages temporal dynamics, a source, and a target SoC estimator to improve prediction

accuracy at ambient temperatures ranging from -20°C to 25°C. The experimental results validate the approach.

The primary method of leveraging transfer learning is one in which there is a source domain with a high number of data points and a target domain with a smaller number of data points. The data representations for both the target and source domains are usually the same although that may not be the case in scenarios where feature extraction is employed. In this thesis, the data representation is images of size 224x224 pixels, the source domain is the ImageNet dataset[43], and the target domain is the voltage curve dataset generated from the full and partial charging voltage curves of cycled lithium-ion batteries. Figure 5.1 illustrates the general transfer learning approach utilized in this thesis.

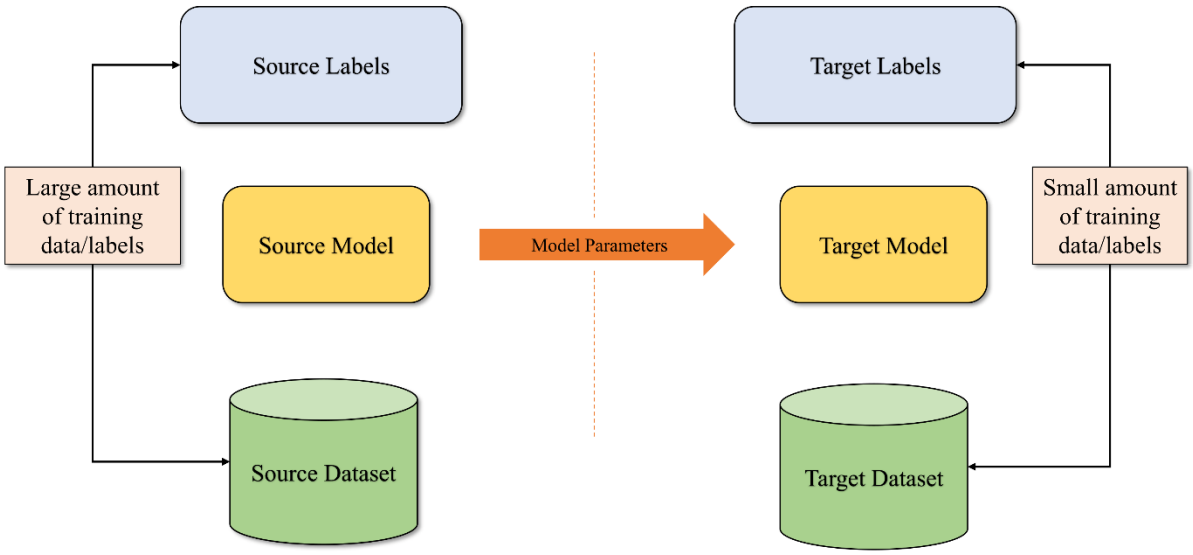

Figure 3.2: Transfer Learning Process

3.4 Summary

In this chapter, the details of the LSTM neural network were discussed followed by a discussion of the internals of CNNs, and then the chapter was wrapped up with a discussion of transfer learning and a brief literature review of relevant publications.

Chapter 4. Methodology

In this chapter, the details of the experiments conducted with the voltage charge curve and voltage charge curve residuals are discussed. Firstly, the experimental setup and induced faults are discussed followed by a discussion of the RES152 network used in both experiments. The voltage monitoring LSTM solution is then discussed followed by a discussion of how the residuals are created, and the chapter ends with a discussion of the various training optimizations performed to enhance the fault classification process.

4.1 Experimental Setup & Induced Faults

A visualization of the entire fault diagnosis process from data collection to results analysis for the voltage charge curves and voltage residual curves are shown in Figures 4.1 and 4.2 respectively. The battery utilized in the training and testing experiment was a commercially available 18650 form factor cell (UR18650AA, Sanyo). It is comprised of a graphite anode and Nickel Manganese Cobalt Oxide (NMC) cathode. The voltage and nominal capacity of the battery are 3.6V and 2.25Ah. The experiment was conducted at 25^{o}C. The specifications of the cell are shown in Table 4.1.

For the first validation set experiment, a new batch of batteries identical to those used in the training/testing experiments were used to create a validation dataset. Another validation set was also created to study the efficacy of the developed technique on different battery chemistries. The battery used for this was another commercially available 18650 form factor battery (LG LGGBF1L1865, LG). It has a similar electrode material pairing as the batteries used for the training/testing experiment and the other validation set.

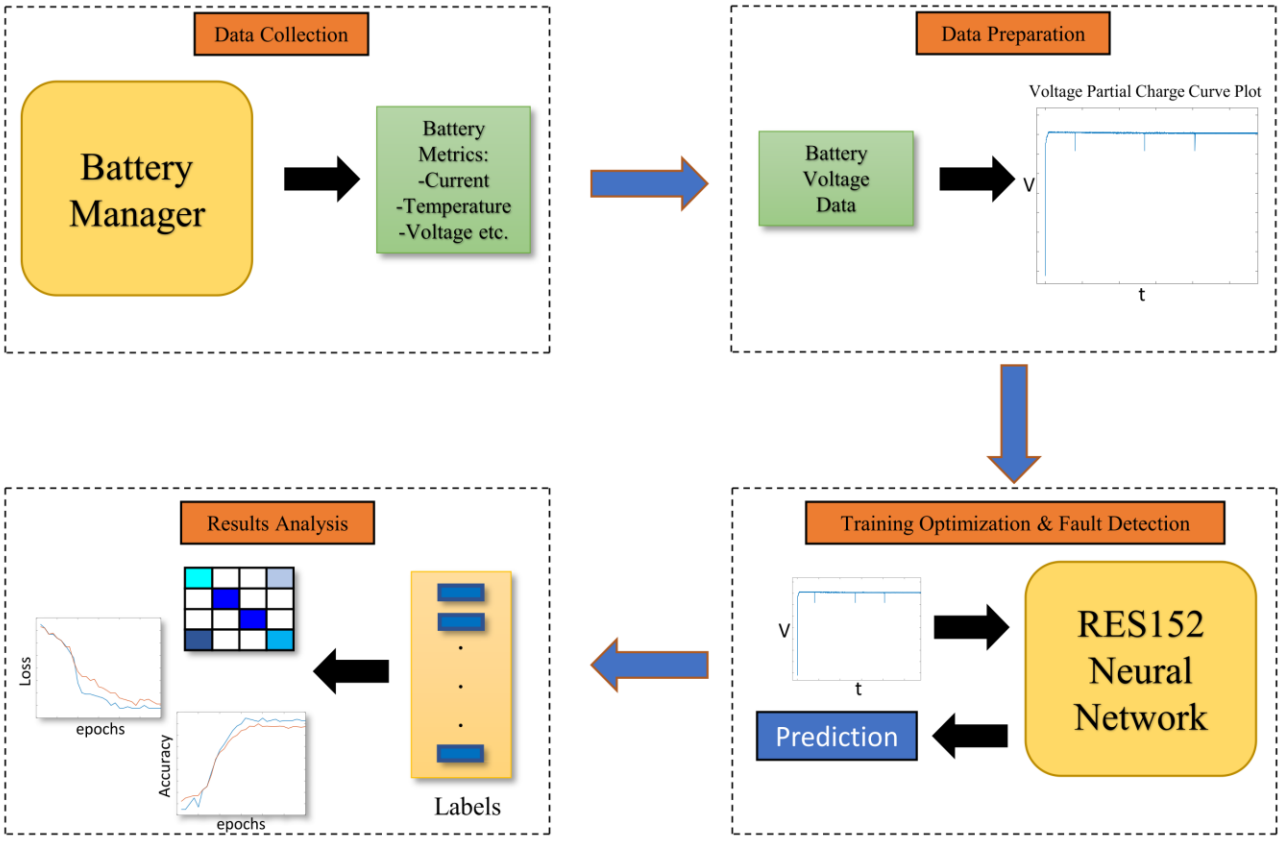

Figure 4.1: Experimental Process Overview (Voltage Charge Curve)

Table 4.1: Specifications of the Training/Testing/ Validation Set 1 Battery

Specifications	Cell
Cell Type	UR18650AA. Sanyo
Electrode Material	Li(Ni0.8Co0.1Mn0.1)O2 / graphite
Nominal Capacity	2.25Ah
Minimum Capacity	2.15Ah
Charge cut-ff voltage	4.2V
Nominal Voltage	3.6V
Discharge cut-off voltage	2.5V
Charge and Discharge cut-off current	0.02C
Standard Charging Current	0.7C

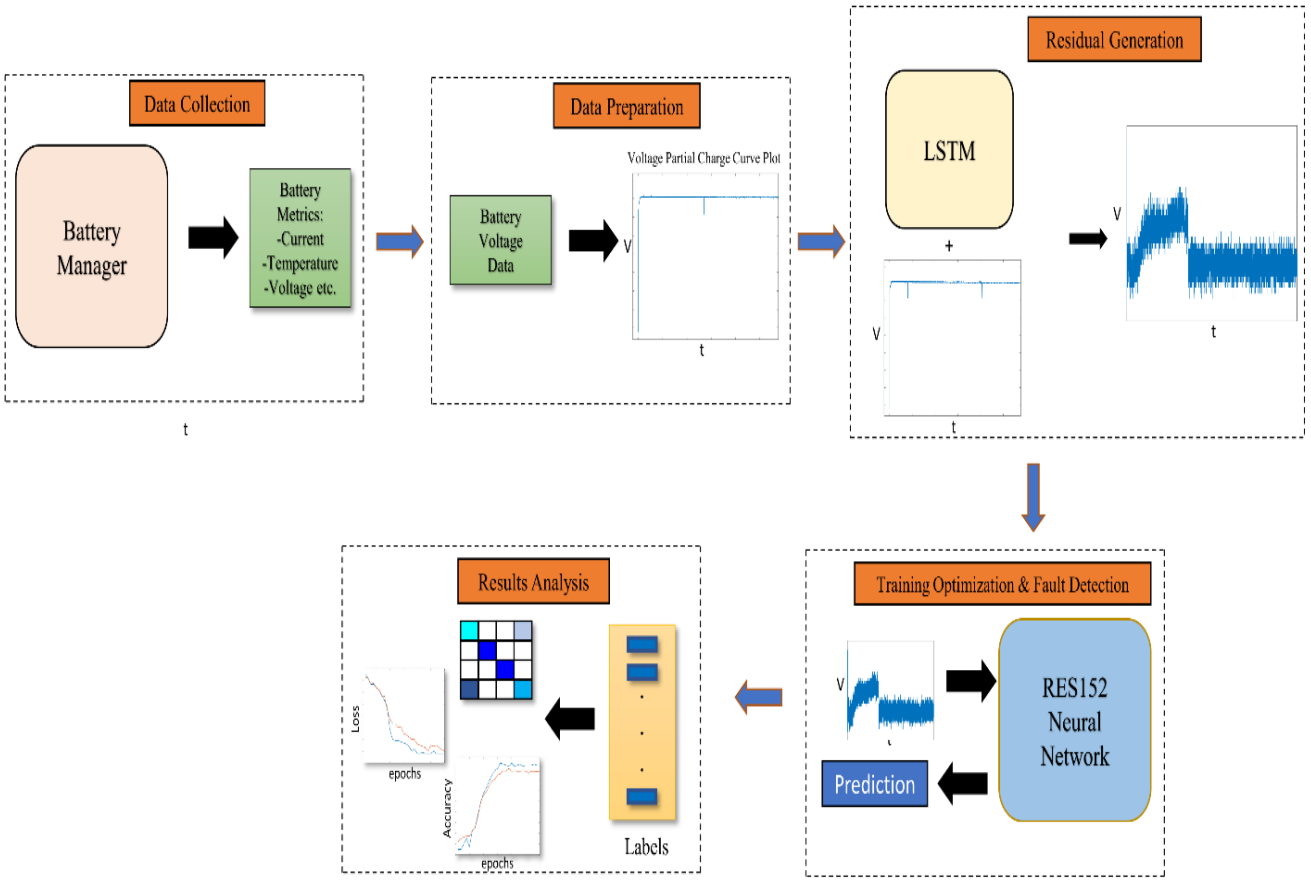

Figure 4.2: Experimental Process Overview (Voltage Residual Curve)

The battery manager used in this experiment is shown in Figure 4.3a. A close-up of the battery along with the thermocouple and heat pad used for inducing faults in the battery is shown in Figure 4.3b. Figure 4.4 shows the schematic for the battery manager. In the experiment, 3 faults are induced in the batteries. These faults are abnormal heating, internal short circuit, and overcharge/overvoltage. There are simpler ways to detect the overcharge fault such as direct measurement; however, in this study, to demonstrate the robustness of this technique to different faults of varying complexity, the overcharge fault was included. Since there is an inbuilt mechanism within most BMS systems, real-world overvoltage faults may not occur, but by training a technique that is capable of detecting this fault, it can act as a second line of defense against the rare occurrence of such a fault. This overvoltage fault detection feature is nice to have but not completely necessary since it is also trained to detect more severe faults such as an internal short circuit. The thermal fault is simulated via a heating pad attached to the cell during charging. The effect of temperature on the internal resistance of a lithium-ion cell is studied in [49]. The researchers found that an increase in temperature would lead to an increase in the ionic conductivity of the cell and conversely a reduction in temperature would lead to a reduction in ionic conductivity. As the thermal fault generates extra heat to the battery cell, the battery temperature increases and the internal resistance of the cell reduces, leading to an accompanying change in the voltage curve. This change is the increase in the time taken to finish the CC (Constant Current) portion of the charging and a slight reduction in the overall voltage due to the lower internal resistance. The use of the external resistor to simulate an internal short circuit is a viable technique employed by other researchers such as in [22].

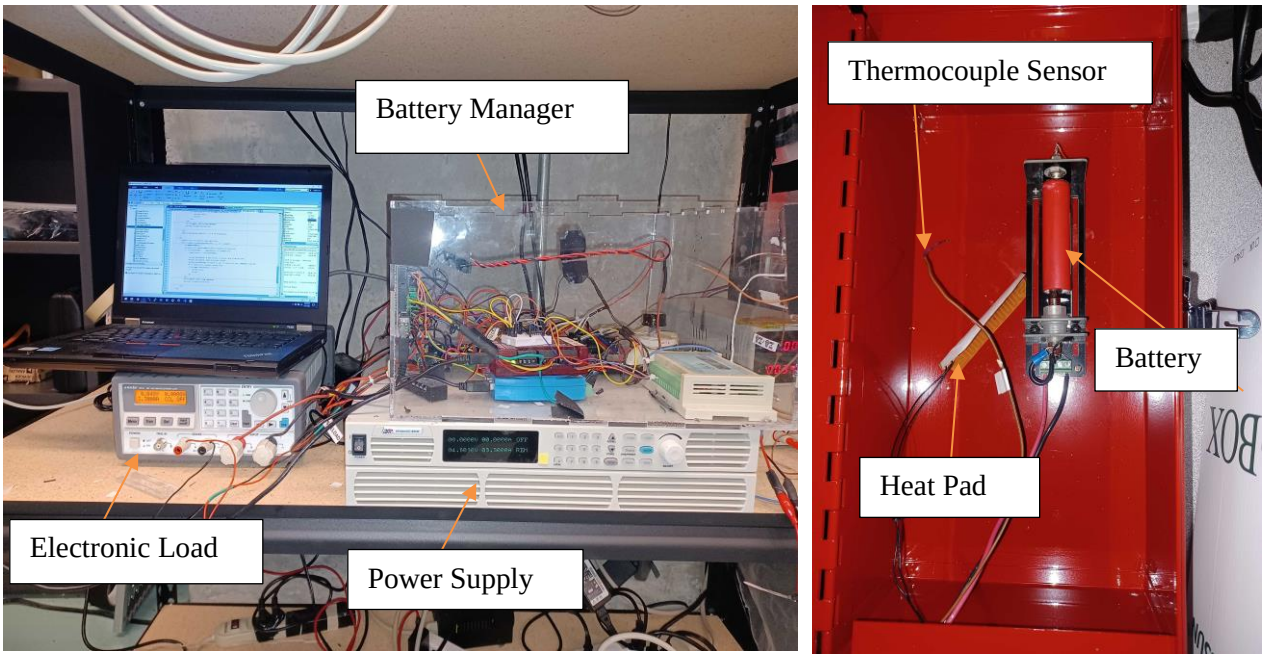

Figure 4.3: a) Battery Manager b) Battery Inside Safety Box

Table 4.2: Types of Faults

Fault	Code	Simulation
Healthy	HEALTHY	Regular operation of the battery
Internal Short Circuit	ISC	1-ohm resistor across battery terminals
Over Voltage	OVERVOLT	Charged 0.4V above cutoff voltage
Abnormal Temperature/Thermal	THERM	Heat pad applies heat directly to the cell

A fourth fault class is also created which is the “Healthy” fault class. Data is obtained for this fault class of the battery under regular operating conditions and this fault class acts as a baseline. A summary of the faults and their method of simulation is shown in Table 4.2.

For each fault, the battery is discharged to a random value between 40-60% SOC and then charged back up to 100% SOC at a rate under 1C under a constant current constant voltage (CCCV) charging protocol. Preliminary studies conducted by the author showed that at lower ranges(0-40% SOC) the network had similar classification ability and so the range of 40-60% was chosen for the experiment. 30 cycles are collected for each fault class. For the creation of the dataset, the partial charging voltage data is plotted and labeled based on the fault class it was created from. The overall dataset consists of 120 images, of which 80% are used for training and 20% are used for validation. Overfitting does not occur because of the train/test split. This is verified via the results of the validation experiments which show similar classification performance. There are 2 validation sets in this experiment created from two different sets of batteries. The first validation set is referred to as “Validation Set 1” and consists of 5 cycles of each fault using the Sanyo batteries. The second validation set, called “Validation Set 2”, is created using the LG batteries and consists of 5 cycles from each fault class.

4.2 RES152

The model used for this study is a pre-trained ResNet 152 (RES152) [50] model, which is part of the CNN family. The main benefit of CNNs is their ability to automatically extract differentiating features from images that are fed into them. Voltage data is used by researchers for fault detection because there is usually an accompanying change in voltage from the traditional state when a fault occurs. If the voltage data is graphed and converted into an image that can be processed by the CNN, then the fault signatures that are present within the voltage data can be extracted automatically and used to differentiate between the different types of faults. This automatic feature detection is one of the advantages of the CNN. Traditional machine learning techniques require the researcher to manually create features and choose the features that best encode the fault information. This process can be tedious and prevents non-experts from being able to use these types of networks. By using a CNN on the graphed voltage data, the most representative features are extracted automatically and used to identify the different types of faults. In this thesis, the last fully connected layer of the RES152 model is randomized, reduced to 4 neurons, and retrained on the battery dataset. A comparative study is conducted to show the performance of the proposed method and to also investigate the effects of transfer learning on neural networks. 4 machine learning algorithms, as well as 4 other neural networks, are compared to RES152. The 4 neural networks used for the study are a randomized ResNet 152 neural network, an artificial neural network with 152 layers and 100 neurons per layer, a pre-trained ResNet 34 neural network, and a randomized ResNet 34 neural network. The 4 machine learning

algorithms compared are support vector machine, decision tree, random forest classifier, and k-nearest neighbor classifier. Table 4.3 provides a detailed view of the parameters chosen for each network. The FastAI [51] python library was used for the neural network implementations while the Sci-kit Learn[52] python library was used for the machine learning algorithm implementations.

4.3 Voltage Monitoring & LSTM Prediction

The goal of the LSTM is to predict the voltage n steps ahead in time, thus allowing for the generation of a healthy voltage path from which the actual faulty voltage path can be compared and subsequently used to generate the voltage residuals. The LSTM is comprised of 2 LSTM layers with 50 and 20 neurons respectively and two fully connected layers with 10 and 1 neurons respectively. The last neuron layer is what produces the predicted voltage value. For the training of the LSTM, 4 Sanyo batteries were cycled 10 times each to collect a total of 40 healthy voltage samples. The first 1000 data points were used as the training data with the remainder of the curve then used for testing. A sliding window technique was used to generate the training data from the 1000 samples via equation (5), where *t* is the current time step, *k* is the offset from the start of the sequence, n is the window size and *V* is the resultant array. The mapping was done where at timestep t the input to the network was the array V with the output being the voltage at time step t+1. The loss metric used was RMSE whose equation is shown in (6), where z is the total number of samples, $\widehat{Y_i}$ is the predicted voltage at timestep *i* and Y_i is the actual voltage value at time step *i*.

$$V = t - k + n \tag{5}$$

$$RMSE = \sqrt{\frac{1}{z}\sum_{i=1}^{z}(\hat{Y}_i - Y_i)^2} \tag{6}$$

Table 4.3: Parameters of Algorithms used in Comparative Study

Algorithm	Algorithm Parameters
RES152	Standard ResNet 152 structure[44], output layer = 4 x 1
RES152R	Standard ResNet 152 structure[44], output layer = 4 x 1, random initialization
RES34	Standard ResNet 34 structure[44], output layer = 4 x 1
RES34R	Standard ResNet 34 structure[44], output layer = 4 x 1, random initialization
ANN152	hidden_layer_sizes = 100 max_iter = 1000 activation = identity learning_rate = constant
Support Vector Machine (SVM)	kernel = poly decision_function_shape = ovr gamma = auto C = 1.0
Random Forest	n_estimators = 100 criterion = gini min_samples_split = 2 min_samples_leaf = 1
k -Nearest Neighbor	n_neighbors = 5 weights = distance algorithm = ball_tree leaf_size = 30
Decision Tree	criterion = gini splitter = best max_depth = none min_samples_split = 2

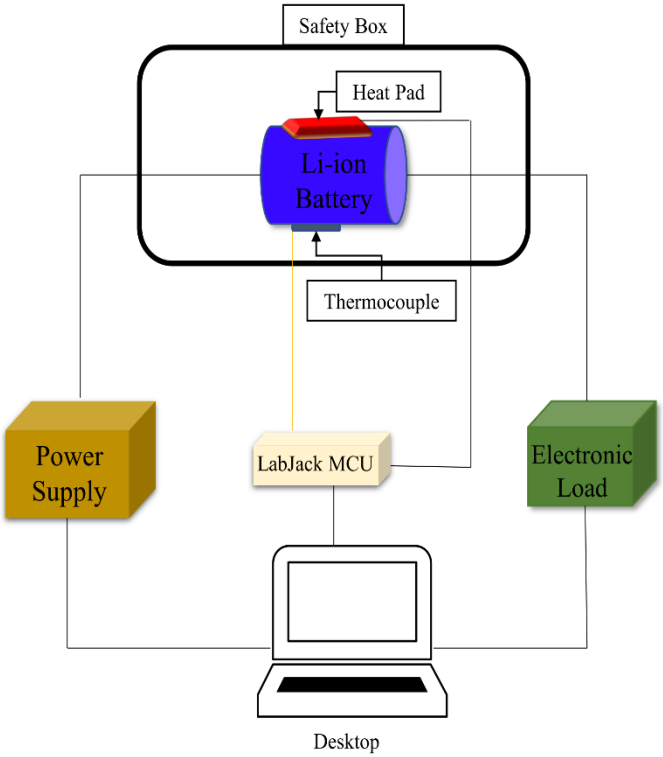

Figure 4.4: Battery Cycler Schematic

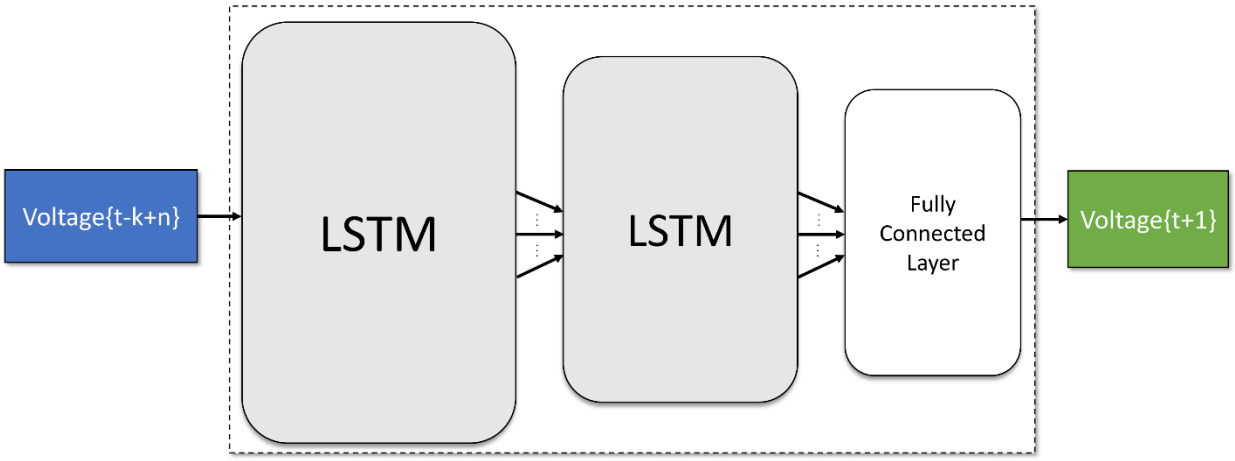

Figure 4.5: Residual Generation Process

4.4 Residual Generation

The voltage residual creation process is shown in Figure 4.5. Once the LSTM has been trained as outlined in section 6.1, the residual is generated according to equation (7), where t is the current timestep, z(t) is the actual voltage at that time step and $\hat{z}(t)$ is the LSTM predicted voltage at that time step. Residuals are generated for all faulty cases and the resultant images are compiled into datasets that are then fed into RES152 for fault classification. Figure 4.12 shows an overlay of the original voltage curve and the prediction output of a trained LSTM.

$$V(t) = z(t) - \hat{z}(t) \tag{7}$$

4.5 Training Optimization & Fault Classification

Figures 4.6 and 4.7 show a detailed view of the RES152 base architecture, with parameters, within the overall fault diagnosis process for the voltage charge curve and voltage residual curve. For the pre-trained RES152 used for this experiment, the last fully connected layer with 1000 nodes is replaced by an identical layer with 4 nodes. This reduction is due to the lower number of fault classes for this experiment. Each node in the final layer corresponds to one fault class. Therefore, since we only have 4 fault classes, the number of nodes has to reduce from the original 1000 count. The source dataset used has 100 fault classes hence the final layer having 10000 nodes The following optimizations were used to augment the training process of the network. Firstly, the image matrices were normalized using the standard deviation and mean value of the ImageNet dataset. This is an important experimental technique to fully

leverage the power of the pre-trained RES152. The normalization scales the pixel values of the images from the battery to an equivalent value on the ImageNet scale. Another optimization as mentioned previously added to the training process was the

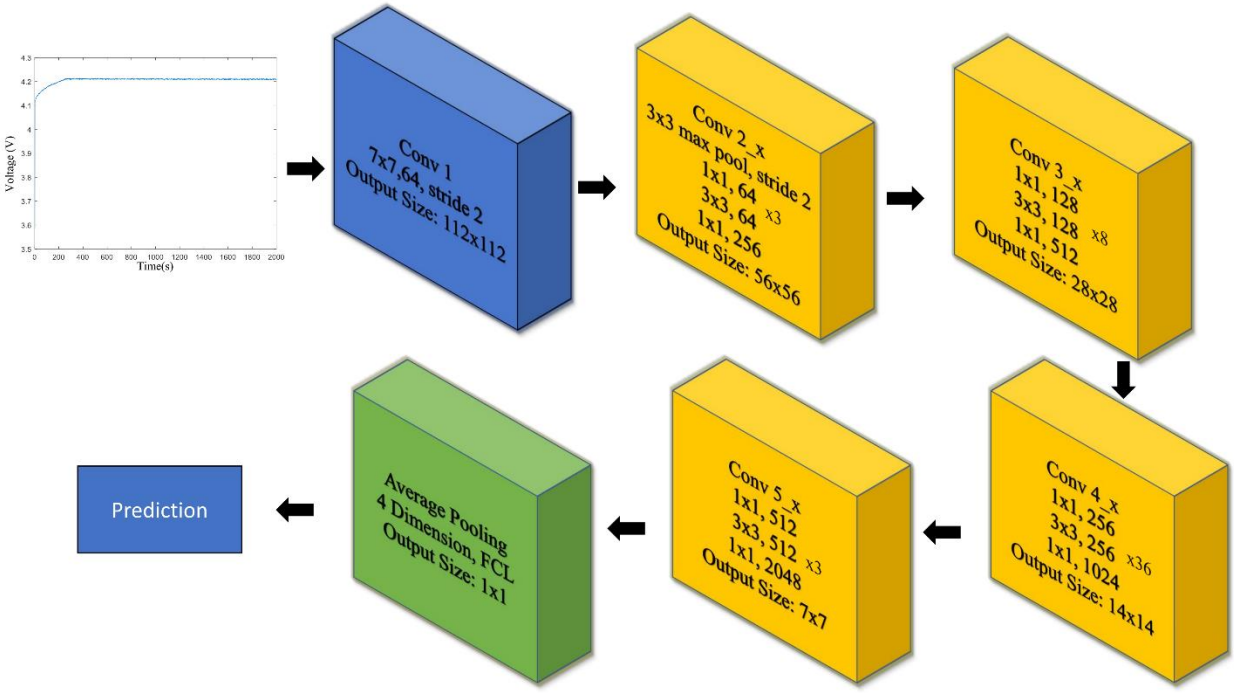

Figure 4.6: Voltage Charge Image Classification Process

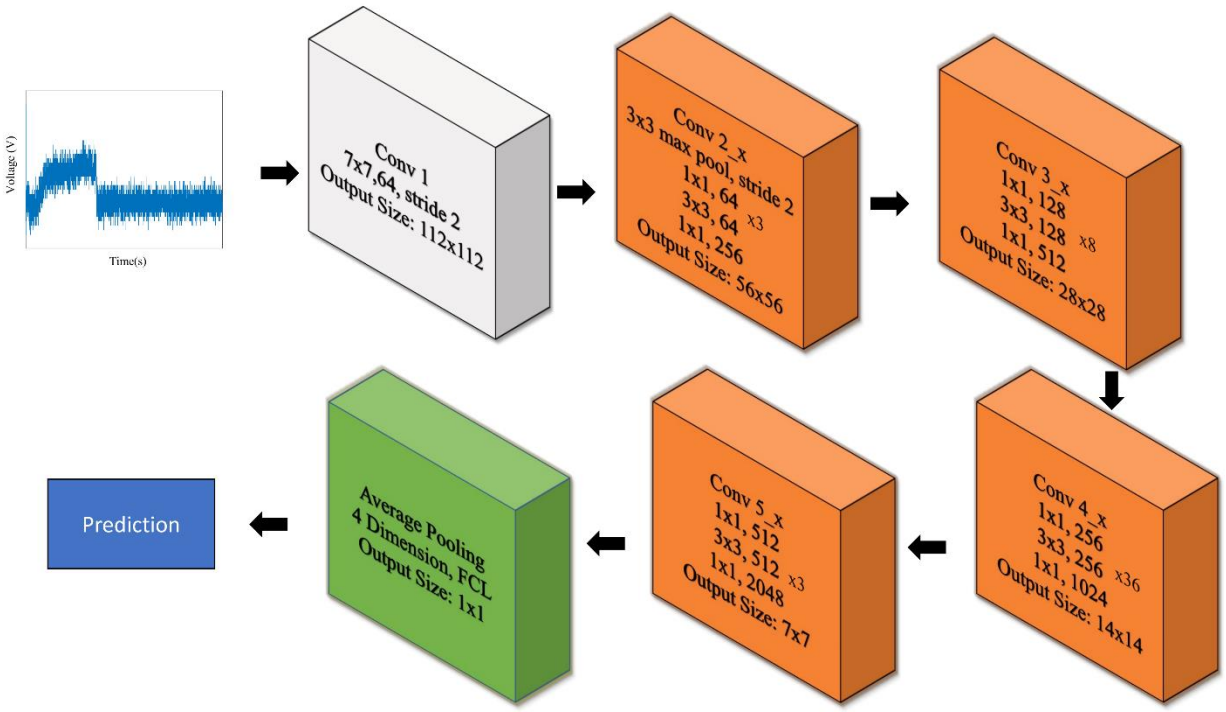

Figure 4.7: Voltage Charge Residual Diagnosis Process

retraining and resizing of the final fully connected layer. The number of layers to retrain on the target dataset is variable in experiments that leverage transfer-learning based networks. As such, it is necessary to derive this information experimentally. Results from a prior experiment on artificially generated battery data as well as preliminary studies on the partial charge dataset both showed the effectiveness of retraining only the final fully connected layer.

A third optimization perfumed was the scaling of the residual images. This was done to increase the similarity between the target dataset and the ImageNet dataset and so the target dataset images(residuals) were scaled to a size of 224x224 pixels. 224x224 pixels is the size of all the images in the ImageNet dataset and so scaling was of benefit to the training process. A fourth optimization employed was the leveraging of cross-validation. Cross-validation involves the rearrangement of the data points contained within the test set and training set to ensure that the network has a chance to "learn" on every instance in the dataset. A 10-fold cross-validation scheme was used for this study. The final optimizations employed were the use of the Adam [50] optimizer and the one-cycle fit policy[51]. The loss function used to tune the parameters of the network is Cross-Entropy Loss. Cross-Entropy Loss allows for the mapping of a prediction probability to each image in the dataset. This allows for the fine-grained fine-tuning of the network's weights and biases to maximize the probability of the correct label for the image. The formula is shown in equation 8. L represents the cross-entropy loss value, i represents an instance in each batch, m represents the number of samples in the batch, y_i represents the actual label of instance i and $\widehat{y_i}$ represents the predicted label of instance i. The error metric used for the analysis of the performance is accuracy. The

formula is shown in equation 9. TP represents the true positives, FP represents the false positives, TN represents the true negatives and FN represents the false negatives. Figures 4.8 – 4.11 feature representative images of the voltage curves of the 4 faults along with a zoomed-in section to show the dynamics of the partial voltage curve during charging.

$$L = -\frac{1}{m}\sum_{i=1}^{m} y_i \log(\hat{y}_i) \tag{8}$$

$$Accuracy = \frac{TP + TN}{TP + TN + FP + FN} \tag{9}$$

4.6 Summary

In this section, the experimental setup and induced fault were introduced and discussed followed by a discussion of the proposed neural network. The LSTM-based solution used for voltage monitoring and prediction were then discussed followed by a presentation of how the residuals are generated. Finally, the various techniques and processes implemented for training optimization are detailed and discussed.

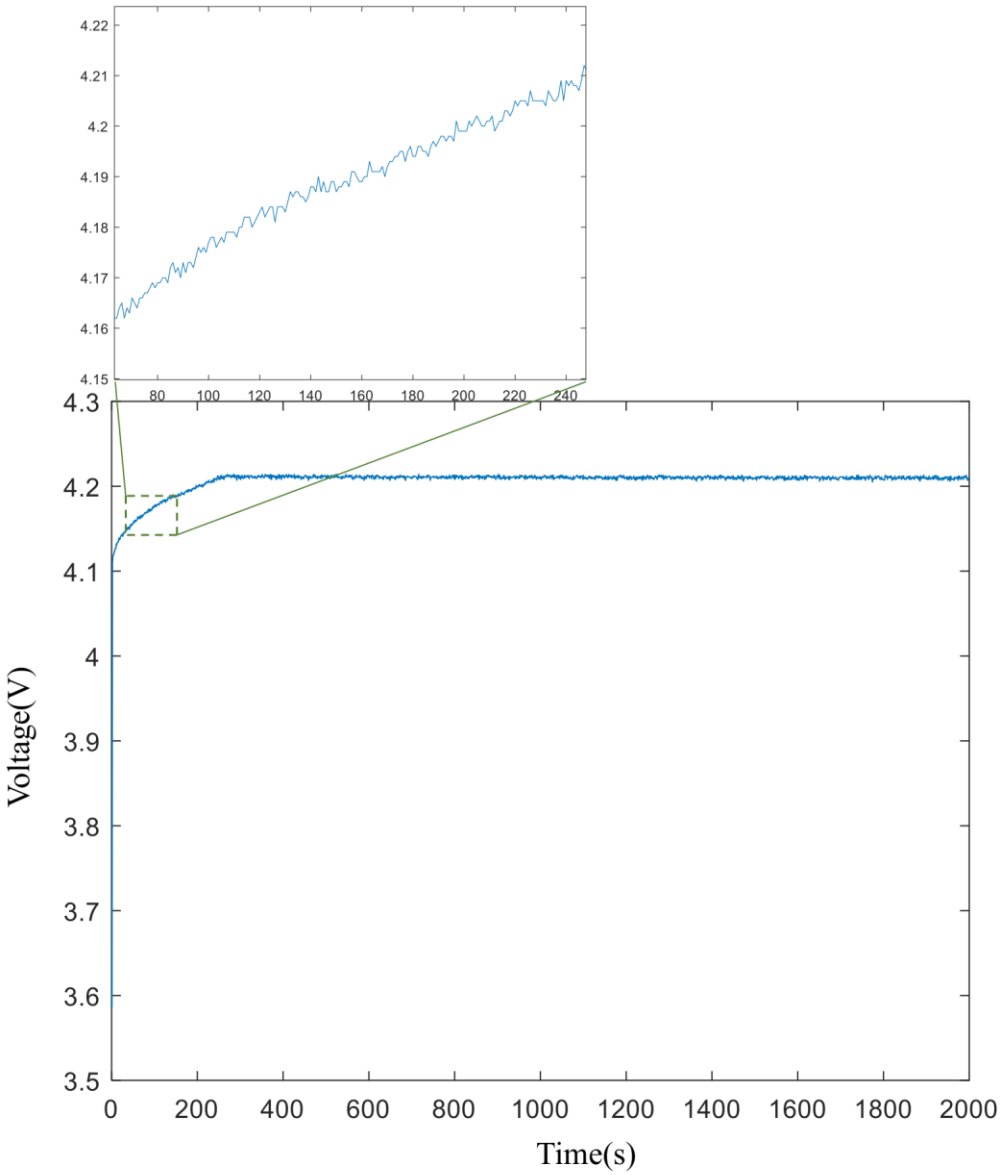

Figure 4.8:HEALTHY Case

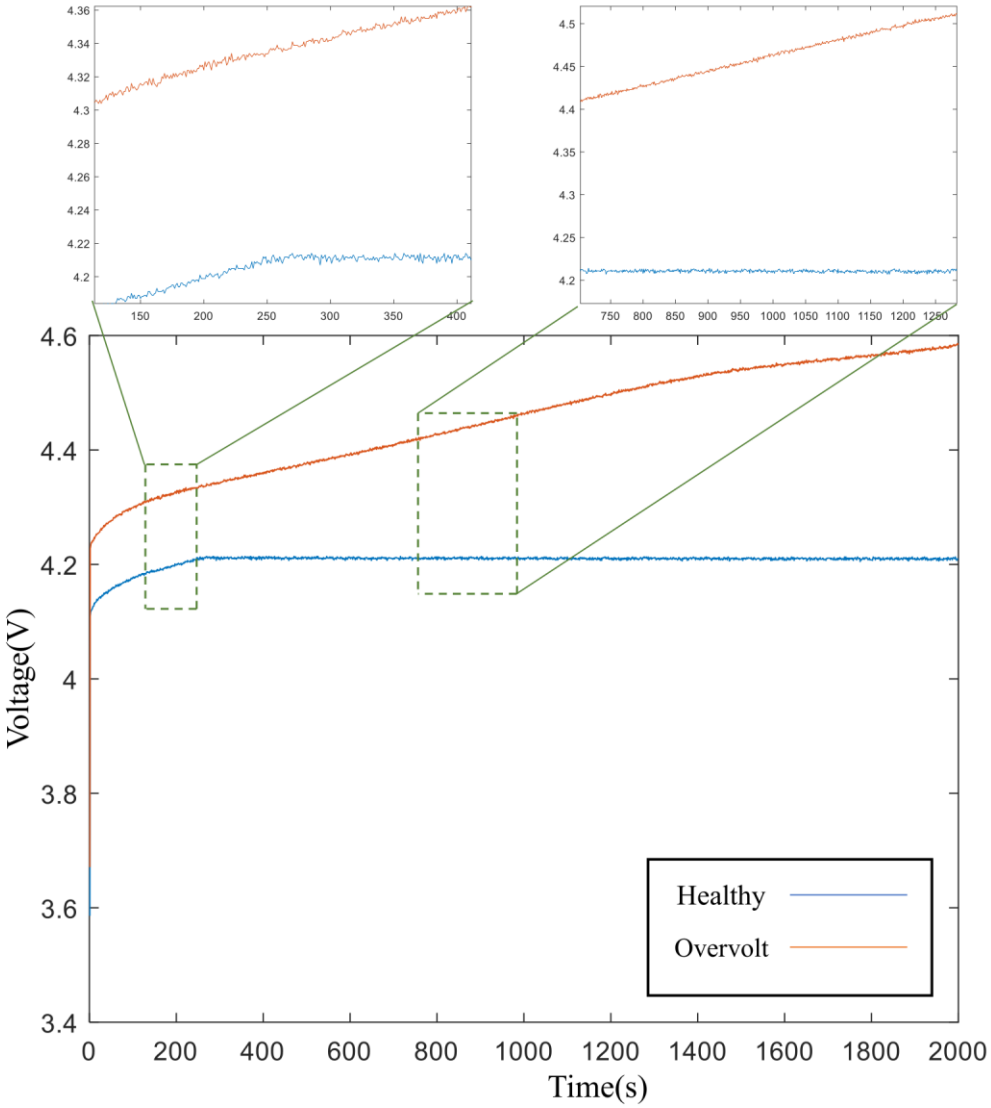

Figure 4.9: Overvolt Fault

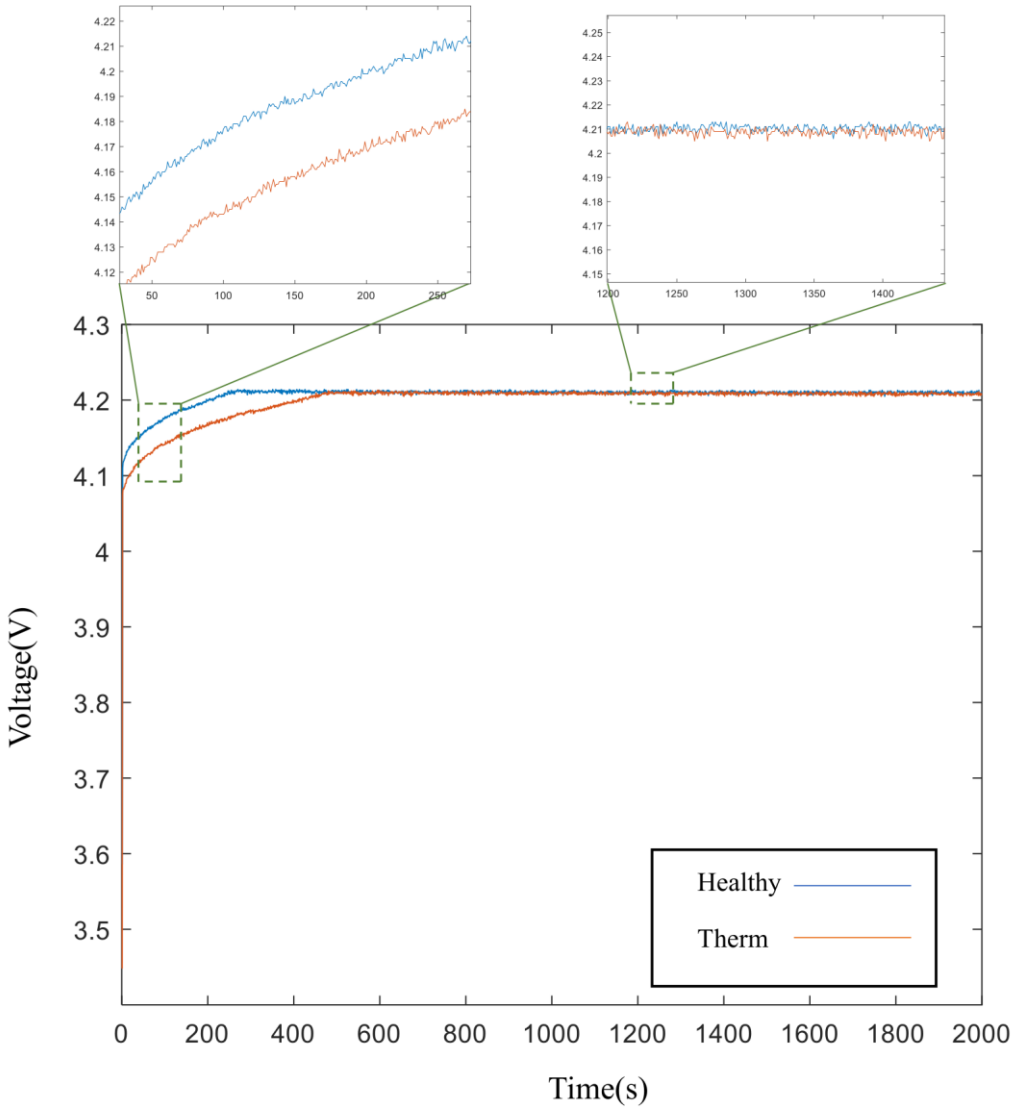

Figure 4.10: THERM Fault

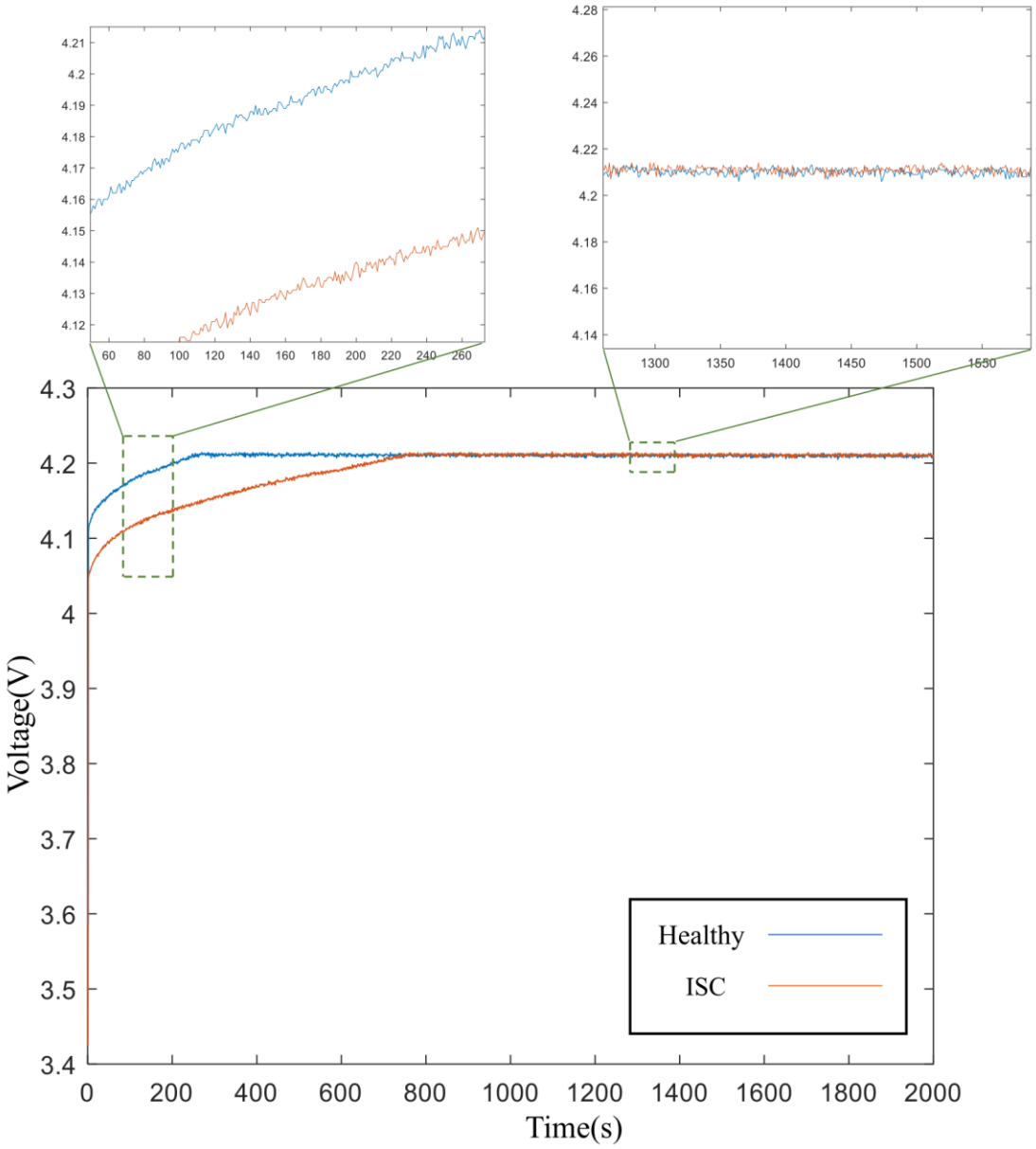

Figure 4.11: ISC Fault

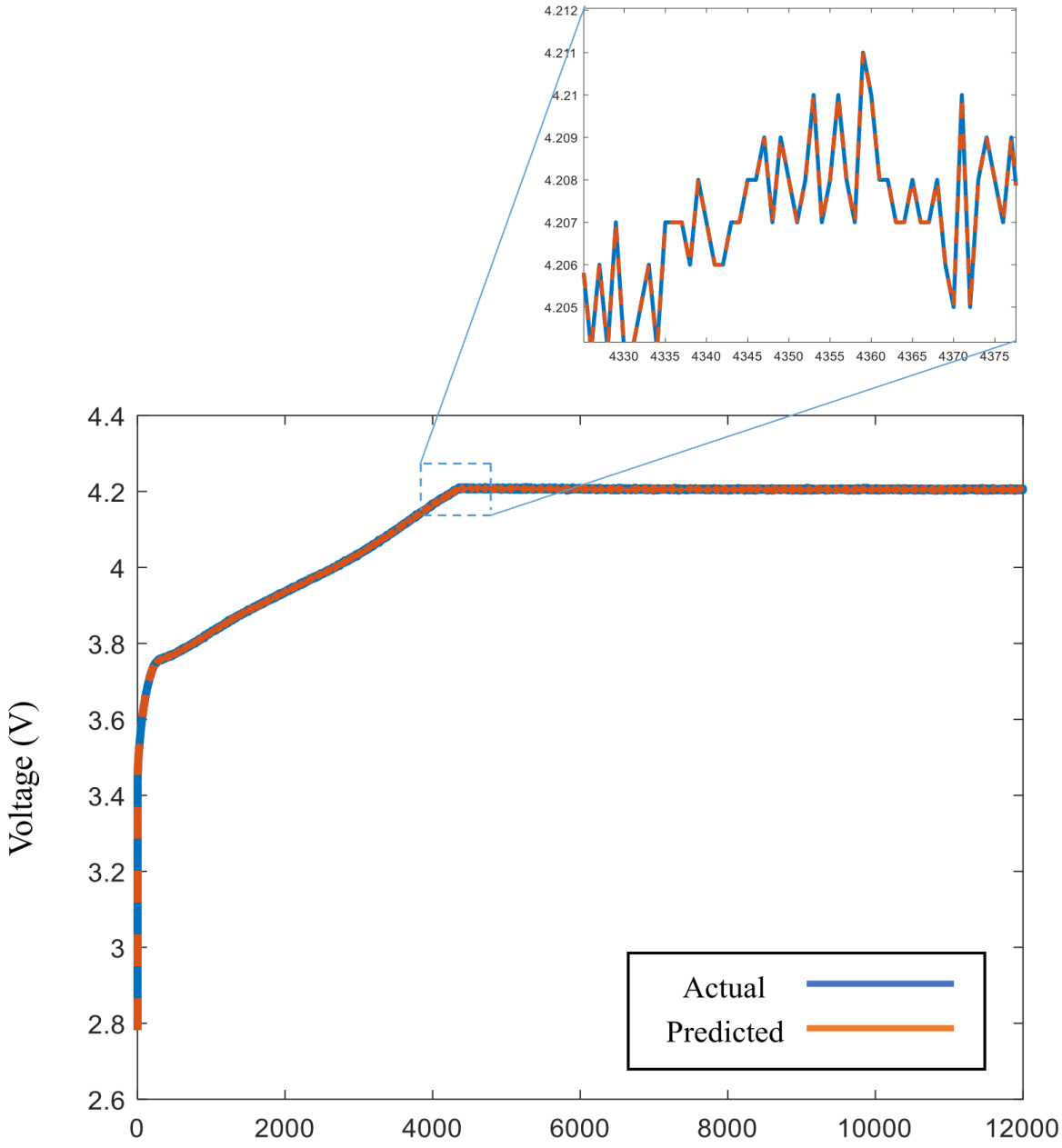

Figure 4.12: Original Voltage Curve + LSTM Predicted Curve

Chapter 5. Results and Discussion

5.1 Introduction

In this section, the results of the fault diagnosis experiments are presented and discussed. Section 5.2 covers the results of the voltage charge curve experiments. Section 5.3 covers the results of the voltage residual curve experiments.

5.2 Experimental Results using Plotted Voltage Charge Curves

In this section, the results of the fault diagnosis exercise on the different datasets are examined. Table 5.1 shows the results of the fault diagnosis study on the LiB dataset. From the stated results, the RES152 model vastly outperforms the other 9 models. Considering that the network only has 24 samples per fault class to learn on and the faults are very mild simulations, its ability to differentiate between the faults is impressive. Both pre-trained networks outperform their fully randomized counterparts. This shows the inherent benefit of pre-training on the domain dataset (ImageNet). As expected, the machine learning algorithms do not perform well due to the small dataset. Also, no feature engineering/creation is performed. The 3x224x224 pixel array for the image is fed directly to the ML algorithms. The lack of feature engineering is another contributing factor to their poor performance since ML algorithms require some sort of feature engineering for them to perform well in such classification tasks.

As previously stated, for the pre-trained networks, only the last fully connected layer is trained on the target dataset (LiB dataset). The lower layers in the RES152 and RES34

models are trained on the domain dataset and what these lower layers in the networks learn how to do is identify patterns of varying difficulty and complexity. Thus, when the last fully connected layer is trained, the pattern recognition ability of the network is maintained and used on the target dataset allowing it to detect patterns/features unique to each fault. For ANN152, the training procedure was capped at 3h when no visible increase in the accuracy had been noticed. Poor performance was expected, especially for such a deep network. Various issues such as the vanishing gradient phenomenon seem to be occurring during the training of the network. It can be hypothesized that the network got stuck in a local minimum despite the training optimization efforts.

Figure 5.1 shows the training and testing progression of the RES152 network. Within 15 epochs, the network is already at a classification accuracy of over 80%. Further training sees this accuracy increase even further before settling after 25 epochs. Figure 5.2 shows the loss progression of RES152 as the network is trained. A similar pattern to the accuracy is formed which is further verification of the correctness of our training process. The loss similarly is nearly minimized after 15 epochs and has completely settled by the 24th epoch.

Figure 5.3 shows the confusion matrix of the testing dataset. For both the OVERVOLT and THERM fault cases, the network shows perfect prediction ability. With regards to the HEALTHY and ISC, the network encounters some difficulty in being able to differentiate between these two fault classes. Further investigation reveals that this confusion is largely due to the mode of simulation of the ISC fault. As previously stated, the ISC fault is simulated via a resistor connected in parallel with the LiB cell and continuously switched on and off as the cell is cycled. The presence of this fault is

less detectable in the first few cycles and to the network, these first few cycles are nearly indistinguishable from the HEALTHY fault case. As such, the network cannot differentiate one case from the other, as evidenced by the results from the confusion matrix. A recommendation for future endeavors with this technique would be the exclusion of the first few cycles for fault classes that may have similar modes of simulation to avoid the issue just discussed.

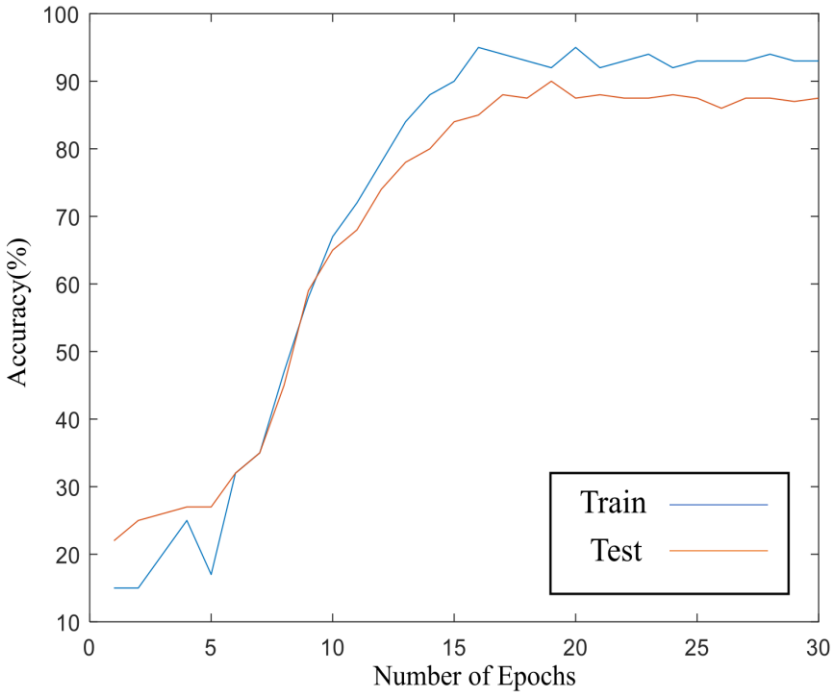

Figure 5.1:Accuracy Plot for Training and Testing Set (Voltage Charge Curve)

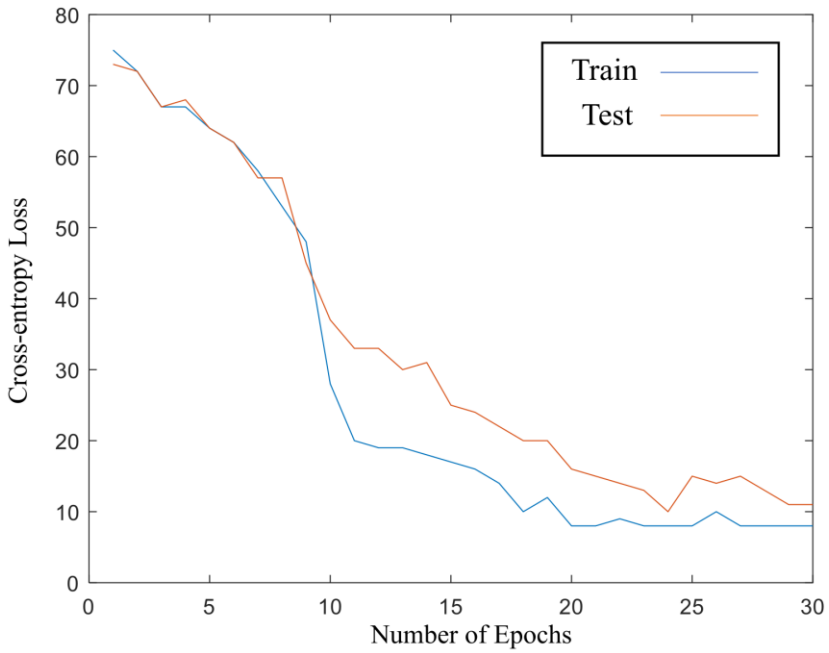

Figure 5.2:Cross-entropy Loss Plot for Training and Testing Set (Voltage Charge Curve)

Table 5.1: Accuracy of Algorithms on Testing Set (Voltage Charge Curve)

Algorithm	Accuracy
RES152	**0.8750**
RES152R	0.4167
RES34	0.6667
RES34R	0.4250
ANN152	0.2500*
SVM	0.2130
Random Forest	0.3200
k -Nearest Neighbor	0.2415
Decision Tree	0.2311

Table 5.2: Training Time of Algorithms (Voltage Charge Curve)

Algorithm	Training Time(s)
RES152	**240**
RES152R	300
RES34	180
RES34R	240
ANN152	10800*
SVM	n/a
Random Forest	n/a
k -Nearest Neighbor	n/a
Decision Tree	n/a

Table 5.3: Accuracy of RES152 on Validation Set 1 & 2(Voltage Charge Curve)

Validation Set	Accuracy
Validation Set 1	85%
Validation Set 2	75%

Table 5.2 shows the training time results for the various networks. The RES34 takes the least time followed by the RES152 network. Both pre-trained networks outperform their fully randomized counterparts as expected due to the reduction in the number of parameters that must be tuned. The ANN152 model as previously stated was capped at 3h due to the lack of accuracy improvement

Table 5.4 shows the accuracy results from both validation sets. As expected, the accuracy for Validation Set 2 is lower than that of Validation Set 1. Validation Set 1 is 2% lower than the test accuracy. It can be reasoned from these results that the network is robust and can perform well on never-before-seen data. Figure 7.4 shows the confusion matrix results for Validation Set 1. The network can accurately identify the ISC and OVERVOLT cases correctly. Like the result of the training exercise, the network struggles with the HEALTHY and THERM classes.

Figure 5.5 shows the confusion matrix of Validation Set 2. The network shows perfect prediction ability for the OVERVOLT case. The network seems to struggle with accurately classifying the other classes correctly. Like the training set and Validation Set 1, the network mistakes the HEALTHY class for the THERM class. However, the network also mistakes the HEALTHY class for the ISC class. It can be inferred from these results that the mode of fault simulation also plays a part in the ability of the network to accurately differentiate between fault classes.

Overall, the RES152 performs well for both datasets given the low data training/testing condition. It has an inference accuracy of 85% for Validation Set 1 and an inference accuracy of 75% for Validation Set 2. These values fall in line with the expected values for this experiment. The batteries used for Validation Set 1 are identical to those used

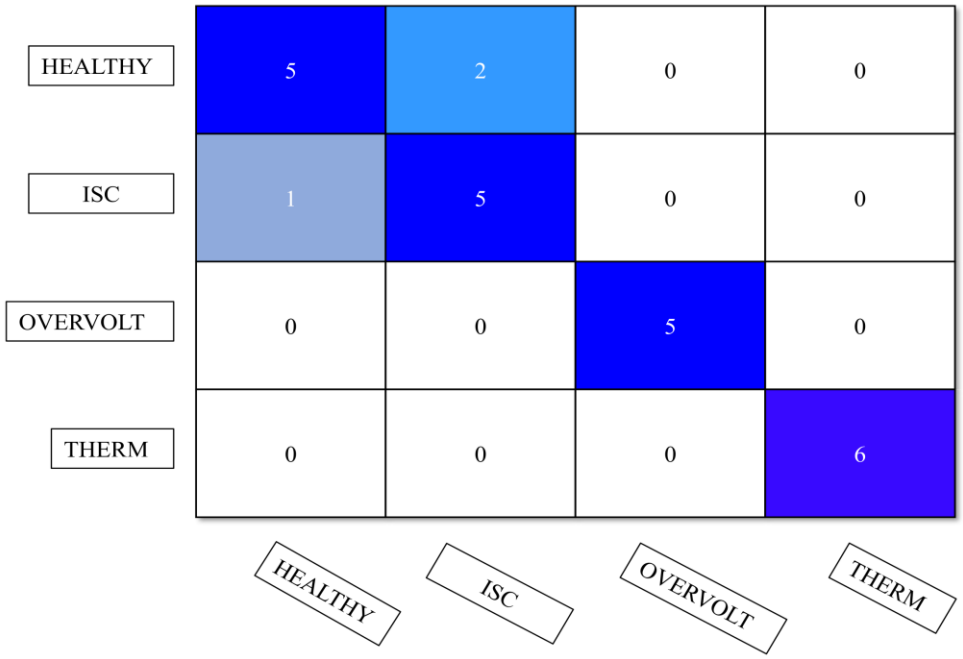

Figure 5.3: Confusion Matrix for the Test Set (Voltage Charge Curve)

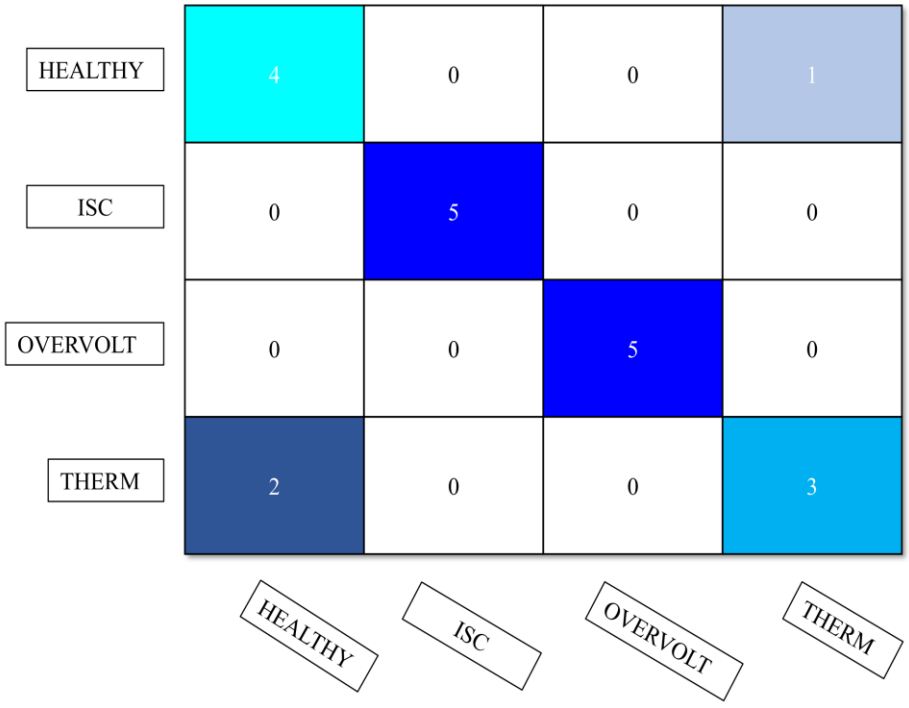

Figure 5.4: Confusion Matrix for the Validation Set 1 (Voltage Charge Curve)

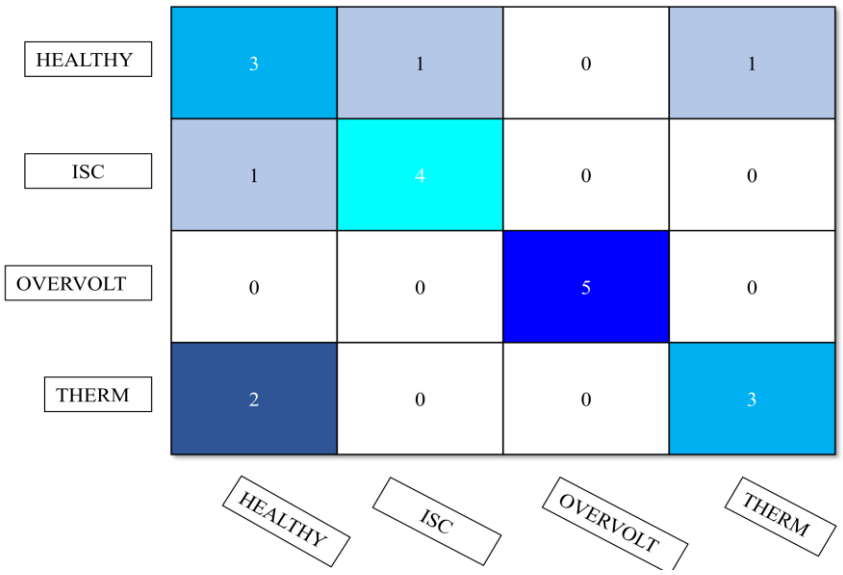

Figure 5.5: Confusion Matrix for the Validation Set 2 (Voltage Charge Curve)

Table 5.4: Accuracy of Algorithms on Validation Set 1 & 2(Voltage Charge Curve)

Algorithm	Validation Set 1	Validation Set 2
RES152	**0.8510**	**0.7530**
RES152R	0.8250	0.7315
RES34	0.8155	0.7125
RES34R	0.7988	0.7010
ANN152	0.2315	0.1255
SVM	0.1800	0.1015
Random Forest	0.2155	0.2102
k -Nearest Neighbor	0.1564	0.1355
Decision Tree	0.1485	0.1025

for the training set and so the network should have similar accuracy to what it had for the testing set. However, Validation Set 2, while having the same electrode materials (NMC/Graphite), is from a different manufacturer. As such different intra-cell reactions are expected compared to the Sanyo batteries and so the expectation is for the RES152 network to struggle more with Validation Set 2.

With regards to the accuracy, Table 5.5 compares the results from [2] and [17] with our technique on all the faults and the short circuit fault in particular. Our technique detects three faults while many other papers only detect one fault(internal short circuit). If we look at the fault detection results of our experiment for only the short circuit fault, we see that the DTL technique achieves 100% accuracy on Validation Set 1. We use Validation Set 1 for comparison because, in the other experiments listed in Table 5.5, their results are reported for a dataset comprised of cycles from the same battery. Validation Set 2 is comprised of voltage cycle data from a completely new battery cell with a different anode/cathode combination and manufacturer. Our results show similar performance to the other listed research when we focus on the fault being detected.

Finally, a practical advantage of this technique is that it can be used where a large amount of faulty data cannot be collected or is not available. By being able to accurately train on a small dataset, the technique can be deployed quickly. Moreover, the technique can adapt and be retrained as more faulty data is collected allowing it to become more robust over time. Also, from our results on Validation Set 2, the technique is capable of detecting faults in other battery chemistries. This would allow for the network to be trained on one battery cell that may have a large amount of faulty data and then be used on another battery that may not have as much faulty data

available. Thus, with this technique it allows for deployment during the early stages. Another contribution of this work is the use of partial voltage curves for fault detection. Most knowledge-based algorithms utilize full voltage charging curves. However, to closer mimic consumer usage of such devices, partial voltage curves were used. The third contribution of this work is the ability of the network to be trained quickly and accurately with a relatively small amount of data(voltage charging cycles). Table 5.5 lists the dataset sizes of similar experiments and shows that our techniques use 8.5 times less data than [2] and 150 times less data than [17] when controlling for the specific fault detected(short circuit). This low data requirement also leads to a short training time. This makes the technique quickly retrainable as new faulty data is obtained. This makes the network more flexible and adaptable, which makes it more useful in real-life scenarios.

5.2.1 Effect of Resistor Value on Fault Detection Capabilities:

To understand the effect of the resistor value on the fault detection capabilities of the RES152 network, cycling data were collected for two other resistors (0.3 ohms and 1.9 ohms). 30 voltage charging cycles were collected for each of the new resistors and the dataset was processed via image dataset techniques from the FastAI library to a final size of 60 cycles, 30 cycles per resistor. A sample voltage plot for all three resistors is shown in Figure 5.6. A similar training and testing methodology as the initial experiment was used for this dataset. The resultant accuracy of the experiment was 99.4% and a confusion matrix is shown in Figure 5.7. We can see from the image that

as we decrease the resistance, the leakage current through the resistor increases, and therefore, the actual charging current to the battery decrease, and the CC portion of the curve increases.

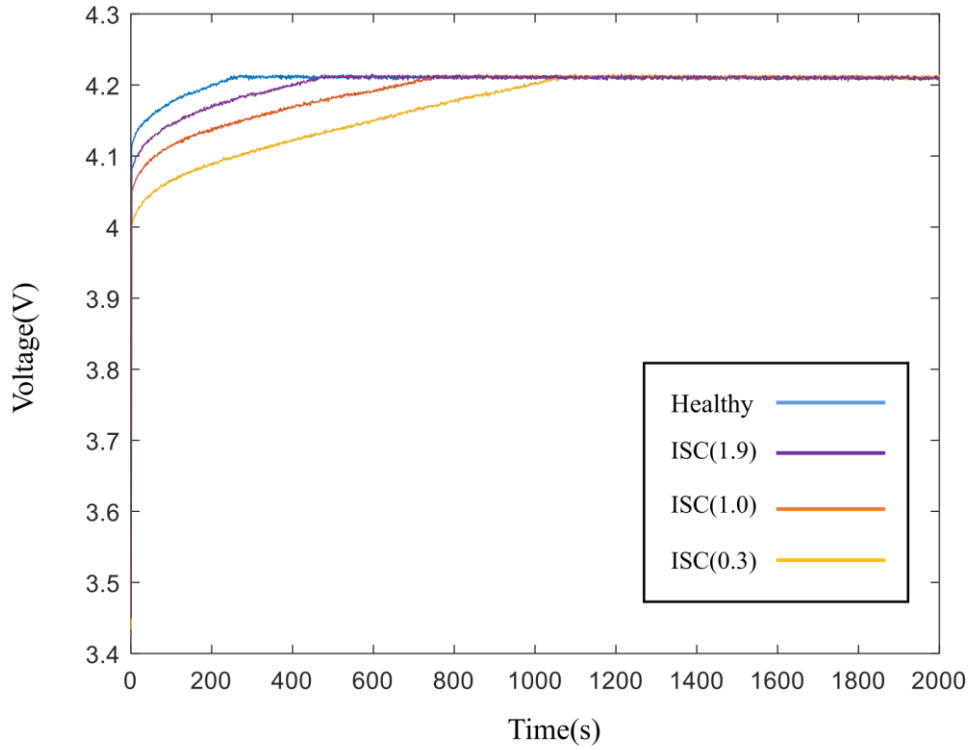

Figure 5.6: Voltage Plot of Internal Shorts

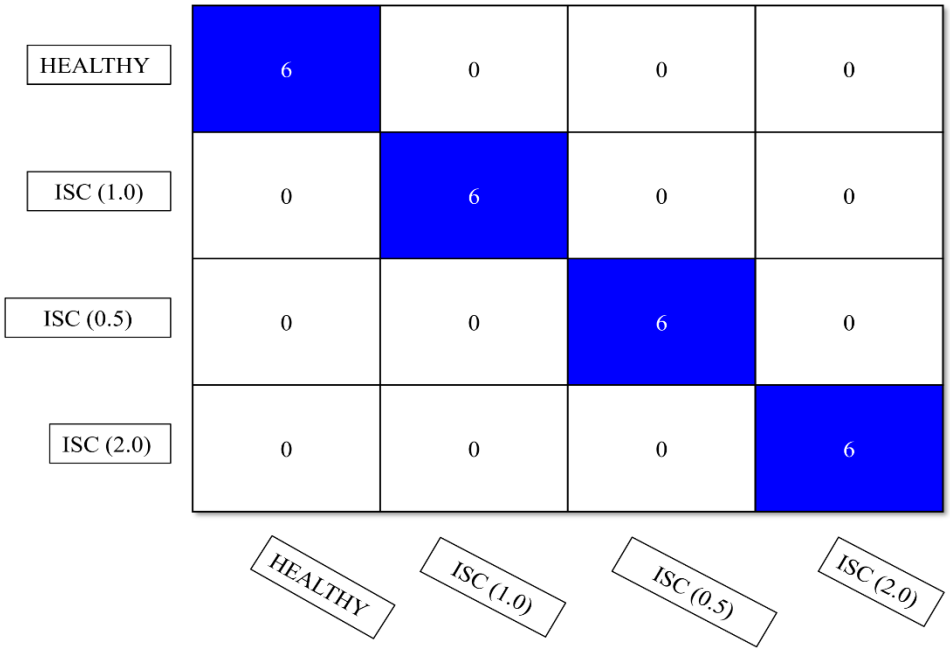

Figure 5.7: Confusion Matrix for Resistor Effect Experiment

Table 5.5: Algorithm Dataset and Accuracy Comparison(Voltage Charge Curve)

Algorithm	No. of Faults	Training Dataset Size(Cycles)	Feature Engineering	Accuracy (%)
RES152	3 (Short Circuit, Overcharge, Thermal)	120	No	91.67
RES152	**1(Short Circuit)**	**40**	**No**	**100.00**
CNN w/ Data Pre-processing[17]-	1(Short Circuit)	6000	Yes	96.00
Supervised Random Forest Classifier[2]	1(Short Circuit)	343	Yes	99.66

5.3 Experimental Results using Plotted Voltage Residuals:

In this section, the results of experiments carried out with the plotted voltage charge residual curves are presented and discussed.

5.3.1 Full Voltage Charging Curves(Randomly Initialized LSTM):

The confusion matrix and accuracy plots for the training and testing datasets are shown in Figures 5.8 and 5.9 respectively. The final accuracy for the validation set is 95% as previously mentioned, the validation set is comprised of 24 samples with each fault class having 8 samples. From the accuracy plot of Figure 5.9, the network seems to achieve 80+% accuracy after just 17 epochs. Further training sees both the training and testing accuracy rise to over 90+% after 30 epochs. In terms of fault misclassification, Figure 5.8 shows that the network mistakes the HEALTHY and THERM faults. Further investigation into this issue leads to the conclusion that the reason may be because of the method of fault simulation during data collection. To simulate a real thermal fault, the amount of heat was varied rather than kept constant. Therefore, in cases where the applied heat was not severe enough, the voltage response may not have been as pronounced as in other cases and so the residual created from the voltage plot would have been quite similar to that of a healthy charge.

A comparative study was also undertaken at this point in the experiment to

Table 5.6: Accuracy of Algorithms on Validation Set(Full Charge)

Algorithm	Accuracy
RES152	**0.9513**
SVM	0.2250
Random Forest	0.3500
k -Nearest Neighbor	0.2565
Decision Tree	0.2441

Table 5.7: Experiments Accuracy Results Summary

Experiment	Dataset	Accuracy(%)
Full Voltage Charging Curves(Randomly Initialized LSTM)	Validation Set	95
Partial Voltage Charging Curves(Randomly Initialized LSTM)	Validation Set 1	89
	Validation Set 2	82
Partial Voltage Charging Curves(Transfer Learning LSTM)	Validation Set 1	94
	Validation Set 2	92

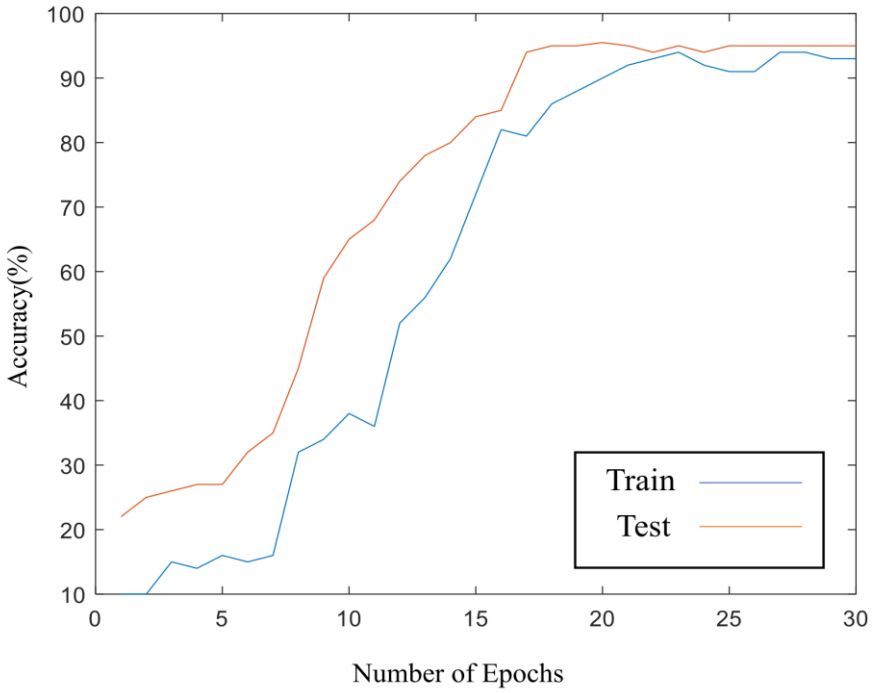

Figure 5.8 : Accuracy Plot, Full Charge, Validation Set (Voltage Residual Curve)

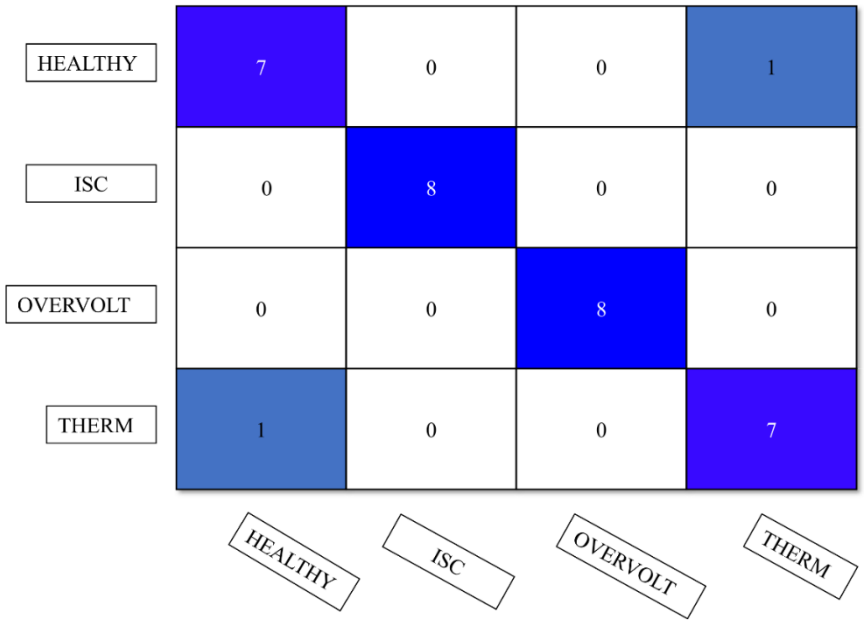

Figure 5.9: Confusion Matrix, Full Charge, Validation Set(Voltage Residual Curve)

benchmark the performance of standard machine learning algorithms against RES152. A summary of the parameters used for the various algorithms in the comparative study is shown in Table 4.3. The results of the classification experiments are shown in Table 5.6. To maintain fairness in terms of access to data, all the machine learning algorithms were trained on the entire dataset (training + test + validation). This was done to ensure that all tested algorithms had processed every data point. RES152 is shown to vastly outperform the other tested algorithms and the machine learning algorithms do not perform well with none of the tested algorithms getting an accuracy of over 60%. One main contributing factor to the poor performance of machine learning algorithms may be the lack of feature engineering.

5.3.2 Partial Voltage Charging Curves (Randomly Initialized LSTM):

The accuracy plot and confusion matrices for this experiment are shown in Figures 5.10, 5.11, and 5.12 respectively. In terms of the accuracy plot, the overall performance is slightly worse than the full charging curve cases discussed above in terms of the overall training and testing accuracy. The network reaches 80+% accuracy after 17 epochs similar to the full charging case. From Table 5.7, the accuracy for validation sets 1 and 2 are 89% and 82% respectively. The batteries used for the validation set from the full charging case and the batteries used in validation set 1 are identical as such the network performance is comparable. However, the drop in the accuracy of the network could be attributed to two factors. Firstly, utilizing, partial charging curves means there is less fault information to extract when the residual is created and so the

resultant residual plot may not be as distinctive. Secondly, the LSTM used to generate the residuals is randomly initialized and so does not benefit from any prior knowledge from the full charging case. Validation set 2 has an even worse accuracy of only 82%. This is expected because the batteries used to create this dataset are different from the validation set 1. Different electrode and anode material combinations will lead to different voltage responses and in turn, will develop varying fault residuals. In light of this phenomenon, the performance of the network is acceptable seeing as it is being used on a dataset from which it has seen no data points during its training and testing. With regards to the confusion matrix of validation set 1, there is a similar phenomenon to the confusion matrix of the full charge validation set. The network is mistaking the HEALTHY and THERM cases which may be a result of the induced fault not being severe enough and so not generating a distinct enough voltage response. From the confusion matrix of validation set 2, again makes a classification mistake between the HEALTHY and THERM cases. However, there is also a case where the network mistakes the ISC case for a HEALTH case. Further investigation leads to the conclusion that the varying voltage response due to differing battery chemistries combined with the lack of training done on this dataset is what lead to this misclassification

5.3.3 Partial Voltage Charging Curves (Transfer Learning LSTM):

The accuracy plot and confusion matrices for this experiment are shown in Figures 5.13, 5.14, and 5.15 respectively. In terms of the accuracy plot, similar to the first two

experiments, the network reaches 80+% accuracy after 17 epochs and in this case, all accuracy metrics outperform the randomly initialized LSTM experiment. For the confusion matrices of validation sets 1 and 2, a trend similar to the previous two experiments starts to develop. For validation set 1, although reduced, there is still a case where the THERM case is mistaken for the HEALTHY case. Moreover, for validation set 2, there is also a case where the ISC case is mistaken for a HEALTHY case. Overall, the network performs better registering a 5% and 10% increase in accuracy for validation set 1 and 2. This lends itself to illustrating the benefits of transfer learning both in terms of the image classification CNN and the voltage prediction LSTM.

Overall, RES152 is able to perform excellently on all datasets registering 85+% accuracy on all validation sets processed. This speaks to the efficacy of transfer learning due to the small training dataset size used for the voltage prediction LSTM training and image classification CNN training.

5.4 Summary

In this chapter, the results from the voltage curve and voltage residual experiments are presented and discussed.

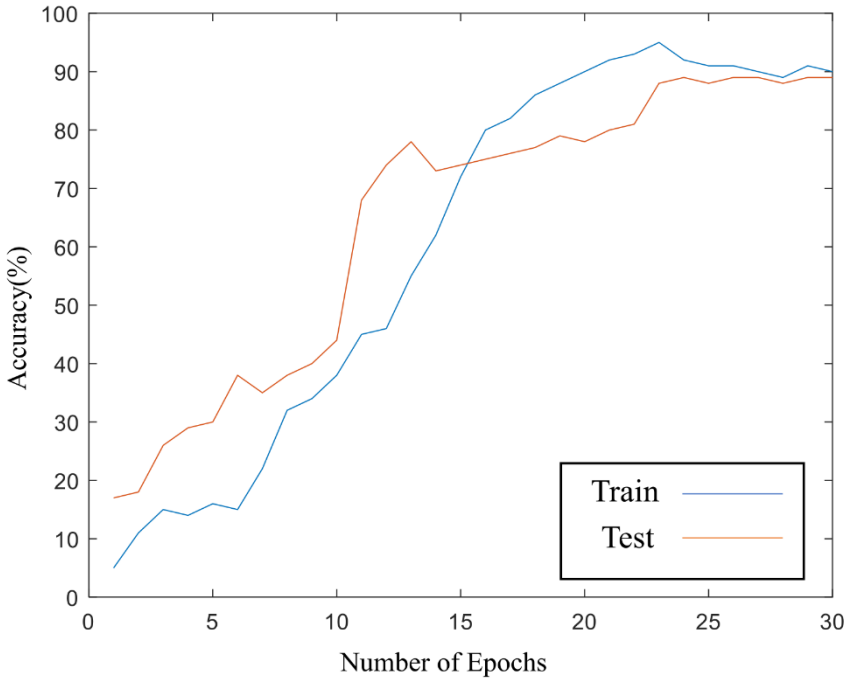

Figure 5.10: Accuracy Plot, Partial Charge(Random Initialization) (Voltage Residual Curve)

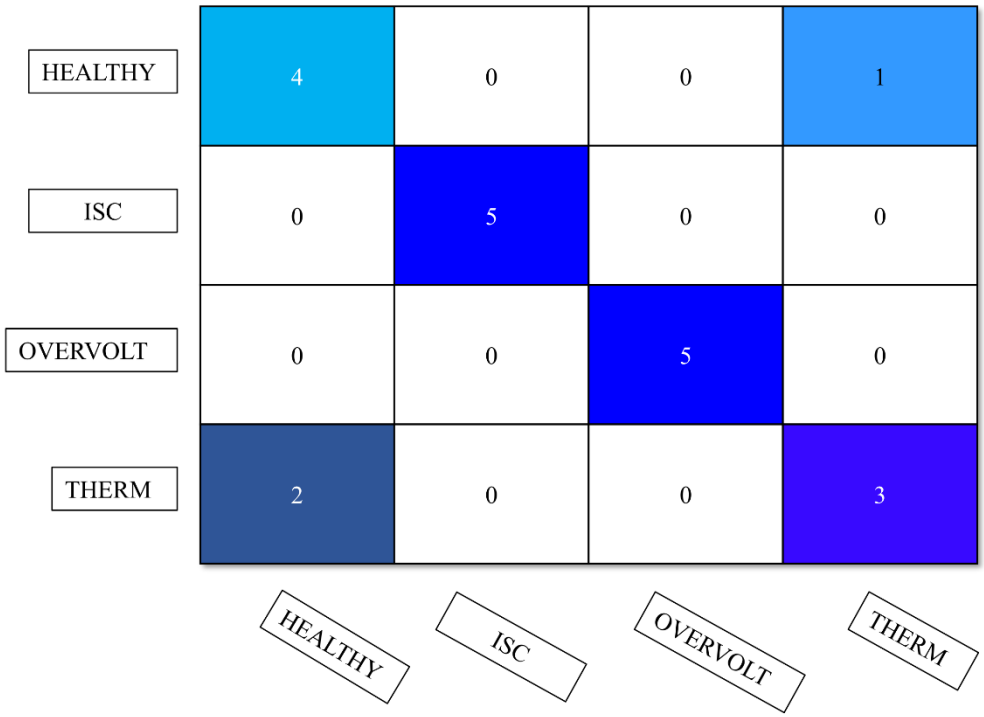

Figure 5.11: Confusion Matrix, Partial Charge(Random Initialization), Validation Set 1 (Voltage Residual Curve)

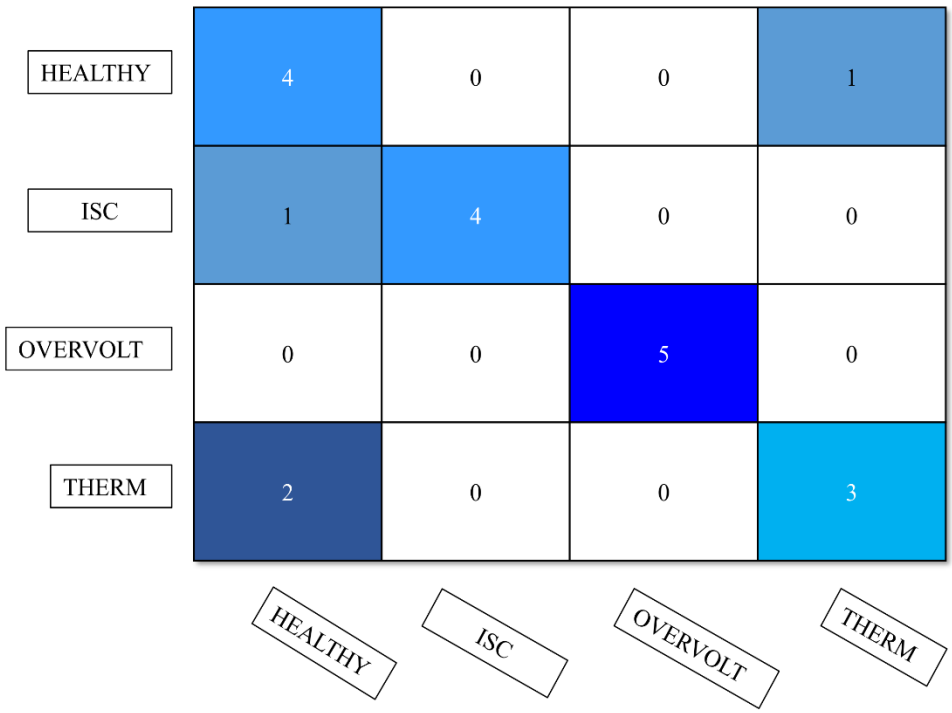

Figure 5.12: Accuracy Plot, Partial Charge(Random Initialization), Validation Set 2(Voltage Residual Curve)

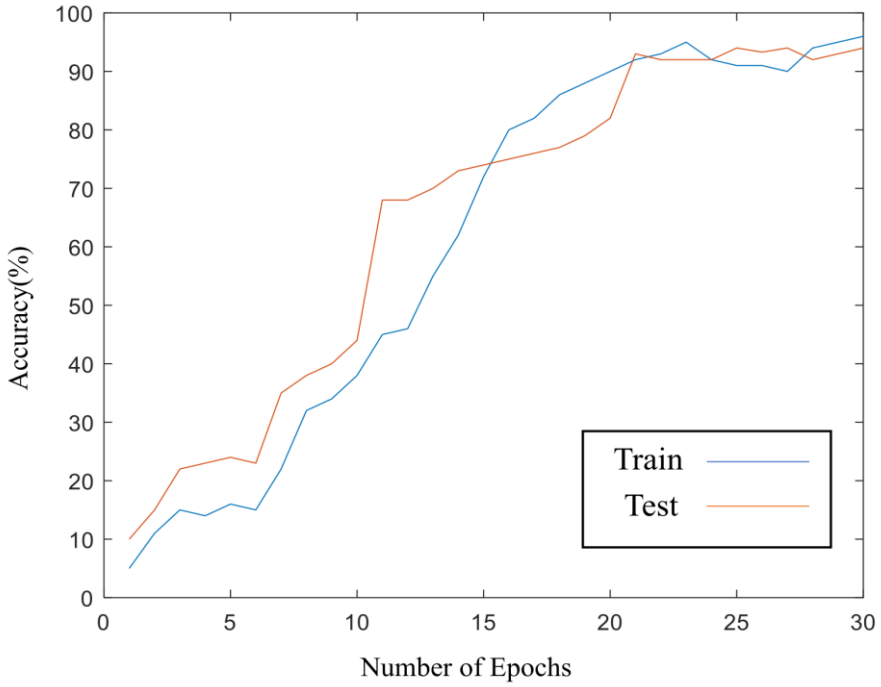

Figure 5.13: Accuracy Plot, Partial Charge (Transfer Learning LSTM) (Voltage Residual Curve)

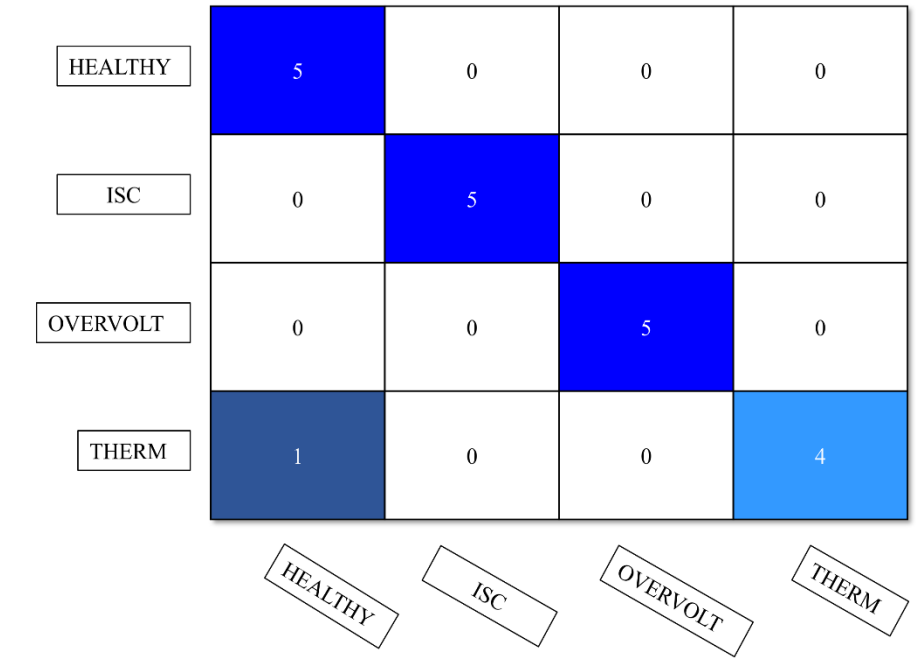

Figure 5.14: Confusion Matrix, Partial Charge (Transfer Learning LSTM), Validation Set 1(Voltage Residual Curve)

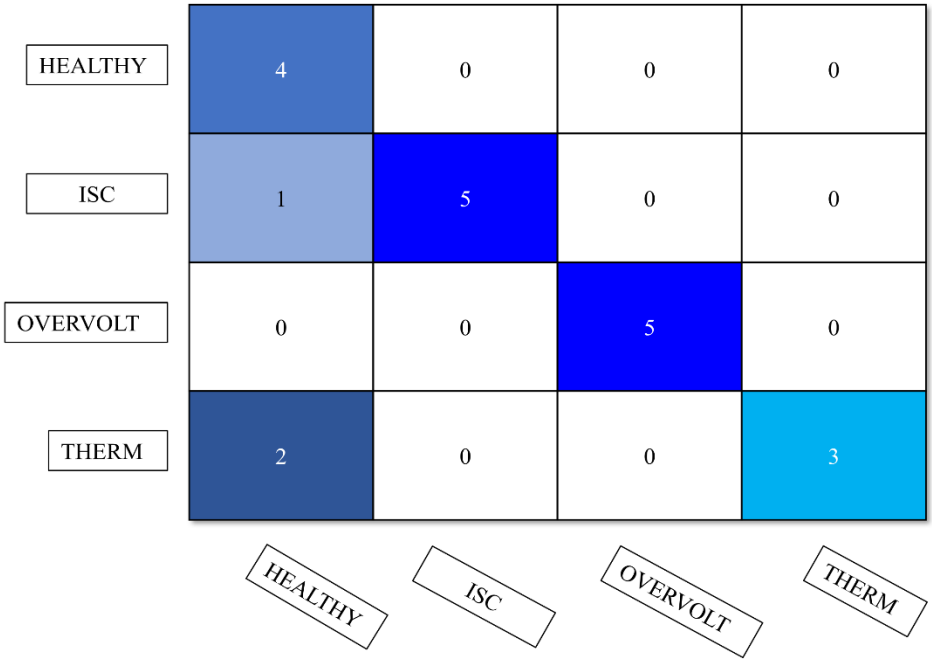

Figure 5.15: Confusion Matrix, Partial Charge (Transfer Learning LSTM), Validation Set 2 (Voltage Residual Curve)

Chapter 6. Conclusion and Future Works

6.1 Conclusion

In this thesis, a ResNet 152 Convolutional Neural Network(RES152) and a 4-layer LSTM neural network are used along with generated voltage residuals to detect faults present within a lithium-ion battery. The developed LSTM-CNN framework was able to accurately detect an internal short circuit fault induced via a resistor, an abnormal heating fault, and an overvoltage fault via the use of voltage residuals. The framework is also able to distinguish a healthy case from the aforementioned induced faults. The fault diagnosis capabilities of the framework are studied for both full charging and partial charging scenarios. The framework is able to achieve a 95% accuracy on the validation set for the full charging voltage curve dataset. For the partial charging voltage curve dataset, the framework is able to achieve an accuracy of 89% and 82% for validations sets 1 & 2 when the LSM is randomly initialized and 94% and 92% when a transfer-learning-based LSTM is used. Overall, the framework performs well in a low data scenario which has long been a criticism of the data-driven techniques. The framework is also adaptable to differing battery chemistries seeing as it is able to achieve 80+% accuracies on a battery dataset from which none of its training samples were derived.

6.2 Future Works

To extend and expound on this research presented, future work to be carried out

includes the expansion of the partial charge range, and inclusion of sensor faults in the faults studied as well as the extension of the framework to work in an online fashion via the use of the LSTM model within the framework. Finally, as the field of image recognition evolves and newer networks like Capsule Networks, which can remember spatial information about the contents of the image, are introduced, the author plans to incorporate such networks into the developed fault detection framework to further improve its efficacy.

References

1. Tran, M. K. & Fowler, M. A review of lithium-ion battery fault diagnostic algorithms: Current progress and future challenges. *Algorithms* **13**, (2020).
2. Seo, M., Goh, T., Park, M. & Kim, S. W. Detection method for soft internal short circuit in lithium-ion battery pack by extracting open circuit voltage of faulted cell. *Energies* **11**, (2018).
3. Hong, J., Wang, Z., Chen, W. & Wang, L. Multi-fault synergistic diagnosis of battery systems based on the modified multi-scale entropy. *Int. J. Energy Res.* **43**, 8350–8369 (2019).
4. Kang, Y., Duan, B., Zhou, Z., Shang, Y. & Zhang, C. Online multi-fault detection and diagnosis for battery packs in electric vehicles. *Appl. Energy* **259**, 114170 (2020).
5. Lin, T., Chen, Z., Zheng, C., Huang, D. & Zhou, S. Fault Diagnosis of Lithium-Ion Battery Pack Based on Hybrid System and Dual Extended Kalman Filter Algorithm. *IEEE Trans. Transp. Electrif.* **7**, 26–36 (2021).
6. Xiong, R., Yang, R., Chen, Z., Shen, W. & Sun, F. Online Fault Diagnosis of External Short Circuit for Lithium-Ion Battery Pack. *IEEE Trans. Ind. Electron.* **67**, 1081–1091 (2020).
7. Li, X. & Wang, Z. A novel fault diagnosis method for lithium-Ion battery packs of electric vehicles. *Meas. J. Int. Meas. Confed.* **116**, 402–411 (2018).
8. Tian, J., Wang, Y. & Chen, Z. Sensor fault diagnosis for lithium-ion battery packs based on thermal and electrical models. *Int. J. Electr. Power Energy Syst.* **121**,

106087 (2020).

9. Liu, Z. & He, H. Model-based sensor fault diagnosis of a lithium-ion battery in electric vehicles. *Energies* **8**, 6509–6527 (2015).

10. Dey, S., Perez, H. E. & Moura, S. J. Thermal fault diagnostics in Lithium-ion batteries based on a distributed parameter thermal model. *Proc. Am. Control Conf.* 68–73 (2017) doi:10.23919/ACC.2017.7962932.

11. Shang, Y. *et al.* A multi-fault diagnosis method based on modified Sample Entropy for lithium-ion battery strings. *J. Power Sources* **446**, 227275 (2020).

12. Liu, Z. & He, H. Sensor fault detection and isolation for a lithium-ion battery pack in electric vehicles using adaptive extended Kalman filter. *Appl. Energy* **185**, 2033–2044 (2017).

13. Ma, M. *et al.* Fault diagnosis of external soft-short circuit for series connected lithium-ion battery pack based on modified dual extended Kalman filter. *J. Energy Storage* **41**, 102902 (2021).

14. Gao, W. *et al.* Micro-short-circuit diagnosis for series-connected lithium-ion battery packs using mean-difference model. *IEEE Trans. Ind. Electron.* **66**, 2132–2142 (2019).

15. Zheng, Y. *et al.* Fault Identification and Quantitative Diagnosis Method for Series-Connected Lithium-Ion Battery Packs Based on Capacity Estimation. *IEEE Trans. Ind. Electron.* **69**, 3059–3067 (2022).

16. Tran, M. K. & Fowler, M. Sensor fault detection and isolation for degrading lithium-ion batteries in electric vehicles using parameter estimation with recursive least squares. *Batteries* **6**, (2020).

17. Nordmann, H., Frisch, M. & Sauer, D. U. Thermal Fault-Detection method and analysis of peripheral systems for large battery packs. *Meas. J. Int. Meas. Confed.* **114**, 484–491 (2018).

18. Zhang, Z., Kong, X., Zheng, Y., Zhou, L. & Lai, X. Real-time diagnosis of micro-short circuit for Li-ion batteries utilizing low-pass filters. *Energy* **166**, 1013–1024 (2019).

19. Lai, X. *et al.* Online detection of early stage internal short circuits in series-connected lithium-ion battery packs based on state-of-charge correlation. *J. Energy Storage* **30**, 101514 (2020).

20. Wei, J., Dong, G. & Chen, Z. Lyapunov-Based Thermal Fault Diagnosis of Cylindrical Lithium-Ion Batteries. *IEEE Trans. Ind. Electron.* **67**, 4670–4679 (2020).

21. Hashemi, S. R. *et al.* A fast diagnosis methodology for typical faults of a lithium-ion battery in electric and hybrid electric aircraft. *Nutr. Today* **17**, 1–8 (2020).

22. Naha, A. *et al.* Internal short circuit detection in Li-ion batteries using supervised machine learning. *Sci. Rep.* **10**, 1–10 (2020).

23. Kang, Y., Duan, B., Zhou, Z., Shang, Y. & Zhang, C. A multi-fault diagnostic method based on an interleaved voltage measurement topology for series connected battery packs. *J. Power Sources* **417**, 132–144 (2019).

24. Li, D., Zhang, Z., Liu, P. & Wang, Z. DBSCAN-Based Thermal Runaway Diagnosis. (2019).

25. Yao, L., Fang, Z., Xiao, Y., Hou, J. & Fu, Z. An Intelligent Fault Diagnosis Method for Lithium Battery Systems Based on Grid Search Support Vector

Machine. *Energy* **214**, 118866 (2021).

26. Wang, Z., Hong, J., Liu, P. & Zhang, L. Voltage fault diagnosis and prognosis of battery systems based on entropy and Z-score for electric vehicles. *Appl. Energy* **196**, 289–302 (2017).

27. Hong, J., Wang, Z. & Yao, Y. Fault prognosis of battery system based on accurate voltage abnormity prognosis using long short-term memory neural networks. *Appl. Energy* **251**, 113381 (2019).

28. Liu, P., Sun, Z., Wang, Z. & Zhang, J. Entropy-based voltage fault diagnosis of battery systems for electric vehicles. *Energies* **11**, (2018).

29. Jiang, L. *et al.* Data-driven fault diagnosis and thermal runaway warning for battery packs using real-world vehicle data. *Energy* **234**, 121266 (2021).

30. Hong, J., Wang, Z. & Liu, P. Big-data-based thermal runaway prognosis of battery systems for electric vehicles. *Energies* **10**, (2017).

31. Zhao, Y., Liu, P., Wang, Z., Zhang, L. & Hong, J. Fault and defect diagnosis of battery for electric vehicles based on big data analysis methods. *Appl. Energy* **207**, 354–362 (2017).

32. Li, D., Zhang, Z., Liu, P., Wang, Z. & Zhang, L. Battery Fault Diagnosis for Electric Vehicles Based on Voltage Abnormality by Combining the Long Short-Term Memory Neural Network and the Equivalent Circuit Model. *IEEE Trans. Power Electron.* **36**, 1303–1315 (2021).

33. Wang, J., Zhang, S. & Hu, X. A Fault Diagnosis Method for Lithium-Ion Battery Packs Using Improved RBF Neural Network. *Front. Energy Res.* **9**, 1–9 (2021).

34. Saeed, U., Lee, Y. D., Jan, S. U. & Koo, I. CAFD: Context-aware fault diagnostic

scheme towards sensor faults utilizing machine learning. *Sensors (Switzerland)* **21**, 1–15 (2021).

35. Yao, L., Xiao, Y., Gong, X., Hou, J. & Chen, X. A novel intelligent method for fault diagnosis of electric vehicle battery system based on wavelet neural network. *J. Power Sources* **453**, 227870 (2020).

36. Zheng, Y. *et al.* Micro-Short-Circuit Cell Fault Identification Method for Lithium-Ion Battery Packs Based on Mutual Information. *IEEE Trans. Ind. Electron.* **68**, 4373–4381 (2021).

37. Samanta, A., Chowdhuri, S. & Williamson, S. S. Machine Learning-Based Data-Driven Fault Detection / Diagnosis of Lithium-Ion Battery : A Critical Review. (2021).

38. Hochreiter, S. & Schmidhuber, J. Long Short-Term Memory. *Neural Comput.* **9**, 1735–1780 (1997).

39. Pascanu, R., Mikolov, T. & Bengio, Y. On the difficulty of training recurrent neural networks. *30th Int. Conf. Mach. Learn. ICML 2013* 2347–2355 (2013).

40. Koushik, J. Understanding Convolutional Neural Networks. (2016).

41. Albawi, S., Mohammed, T. A. M. & Alzawi, S. Layers of a Convolutional Neural Network. *Ieee* 16 (2017).

42. Krizhevsky, A., Sutskever, I. & Hinton, G. E. ImageNet Classification with Deep Convolutional Neural Networks Alex. *NeurIPS* 1–1432 (2012) doi:10.1201/9781420010749.

43. Russakovsky, O. *et al.* ImageNet Large Scale Visual Recognition Challenge. *Int. J. Comput. Vis.* **115**, 211–252 (2015).

44. Zhuang, F. *et al.* A Comprehensive Survey on Transfer Learning. *Proc. IEEE* **109**, 43–76 (2021).

45. Peirelinck, T. *et al.* Transfer learning in demand response: A review of algorithms for data-efficient modelling and control. *Energy AI* **7**, 100126 (2022).

46. Che, Y., Deng, Z., Lin, X. & Hu, L. Predictive Battery Health Management With Transfer Learning and Online Model Correction. *Ieee Trans. Veh. Technol.* **70**, 1269–1277 (2021).

47. Ma, J. *et al.* A hybrid transfer learning scheme for remaining useful life prediction and cycle life test optimization of different formulation Li-ion power batteries. *Appl. Energy* **282**, 116167 (2021).

48. Qin, Y., Adams, S. & Yuen, C. Transfer Learning-Based State of Charge Estimation for Lithium-Ion Battery at Varying Ambient Temperatures. *IEEE Trans. Ind. Informatics* **17**, 7304–7315 (2021).

49. Ma, S. *et al.* Temperature effect and thermal impact in lithium-ion batteries: A review. *Prog. Nat. Sci. Mater. Int.* **28**, 653–666 (2018).

50. He, K., Zhang, X., Ren, S. & Sun, J. Deep residual learning for image recognition. *Proc. IEEE Comput. Soc. Conf. Comput. Vis. Pattern Recognit.* **2016-Decem**, 770–778 (2016).

51. Howard, J. & Gugger, S. Fastai: A layered api for deep learning. *Inf.* **11**, 1–26 (2020).

52. Pedregosa, F. *et al.* Scikit-learn: Machine Learning in Python. *J. Mach. Learn. Res.* **12**, 2825–2830 (2011).